NATIONAL ADVISORY COMMITTEE FOR AERONAUTICS

TECHNICAL NOTE 3874

EXPERIMENTAL AND PREDICTED LATERAL-DIRECTIONAL DYNAMIC-RESPONSE CHARACTERISTICS OF A LARGE FLEXIBLE 35° SWEPT-WING AIRPLANE AT AN ALTITUDE OF 35,000 FEET

By Stuart C. Brown and Euclid C. Holleman

Ames Aeronautical Laboratory
Moffett Field, Calif.

NACA
Washington
December 1956

NATIONAL ADVISORY COMMITTEE FOR AERONAUTICS

TECHNICAL NOTE 3874

EXPERIMENTAL AND PREDICTED LATERAL-DIRECTIONAL DYNAMIC-RESPONSE CHARACTERISTICS OF A LARGE FLEXIBLE 35° SWEPT-WING AIRPLANE AT AN ALTITUDE OF 35,000 FEET

By Stuart C. Brown and Euclid C. Holleman

SUMMARY

The lateral-directional dynamic-response characteristics of a large flexible airplane are presented for flight conditions of 0.6 to 0.82 Mach number and an altitude of 35,000 feet. Transient responses at various stations on the airplane to aileron and rudder pulse-type disturbances have been recorded and converted into frequency-response form. A frequency range of 0.5 to 25 radians per second is presented, which includes the Dutch roll and rolling modes and also three structural modes. The measured frequency responses are compared with those obtained from transfer functions based on the lateral-directional equations of motion, which include first-order effects of structural deflections. Reasonably good agreement is obtained in the low frequency range corresponding to the lateral-directional modes. However, in the higher frequency range, the effects of the structural modes are sufficiently large so that these predictions become inadequate even for the quantities measured near the center of gravity. Comparisons are also made with frequency responses obtained from transfer-function coefficients calculated for the rigid airplane to indicate the effects of flexibility.

Calculated simplified transfer-function coefficients based on the lateral-directional equations of motion are compared with coefficients obtained by matching transient time histories with an analog computer. Aerodynamic derivatives extracted from measured transfer-function coefficients are also compared with estimated derivatives. In general, good agreement between measured and estimated values was obtained.

INTRODUCTION

Because of the increased importance of structural flexibility on aircraft stability, control, and loads, the NACA is currently flight testing a large flexible 35° swept-wing airplane over its entire operating

range of flight conditions. One phase of this program is to investigate characteristics of the airplane dynamic response to control-surface motions. Some results for the longitudinal case and a limited amount of data for the lateral-directional case were presented in references 1 and 2. In a separate investigation, reference 3, some measured frequency-response data were also reported. The purpose of the present report is to present a more detailed description of the lateral-directional characteristics of the airplane at an altitude of 35,000 feet.

The dynamic-response characteristics can usually be separated into the relatively low frequency lateral-directional modes and the higher frequency structural modes. The lateral-directional modes are of primary importance in defining stability and control characteristics of the airplane as a whole, while the structural modes are of importance in the stability of the structure by itself or in combination with an automatic control system (flutter). In the present report, the experimental response over the low frequency range is compared with the predicted responses of the airplane with pseudostatic effects of flexibility included. Predicted responses of the rigid airplane are shown to indicate the effects of flexibility. The measured dynamic response is also examined over the higher frequency range to investigate effects of the first three structural modes.

With regard to measuring and analytical techniques, the frequency response is a convenient way of expressing the dynamic-response characteristics in a standard manner which is independent of the particular input from the control surface. Transient responses to pilot-applied pulse inputs through the rudder or aileron control systems were measured and transformed to frequency-response form by means of the Fourier integral (e.g., ref. 4). While the frequency response represents the dynamic characteristics of the airplane, a sometimes more useful form for the analysis and synthesis of automatic control systems is the transfer function. For the present investigation, transfer-function coefficients obtained from the lateral-directional three-degree-of-freedom case were evaluated by matching time histories on an analog computer in a manner similar to that described in reference 4. Corresponding predicted transfer-function coefficients were calculated, with the coefficients modified to include flexibility effects, and are compared with the experimental values.

The measured transfer-function coefficients usually must be extrapolated to different flight conditions. Since this extrapolation can be done more easily in terms of the aerodynamic derivatives, it is desirable to reduce the transfer-function coefficients to derivative form wherever possible. Accordingly, aerodynamic derivatives obtained from simplifications of the principal transfer-function coefficients are compared with estimated derivatives.

The data used in this report were obtained by the High-Speed Flight Station of the NACA as part of the cooperative program with the Ames Aeronautical Laboratory.

NOTATION

A	aspect ratio
C_L	lift coefficient
C_l	rolling-moment coefficient
C_n	yawing-moment coefficient
C_Y	side-force coefficient
D	differential operator, $\frac{d}{dt}$
I_X	moment of inertia about the X axis, slug-ft^2
I_{X_F}	effective rolling moment of inertia for flexible airplane, $I_X - q_o SbC_{l_{\ddot{\varphi}}}$, slug-ft^2
I_Z	moment of inertia about the Z axis, slug-ft^2
I_{Z_F}	effective yawing moment of inertia for flexible airplane, $I_Z - q_o SbC_{n_{\ddot{\psi}}}$, slug-ft^2
I_{XZ}	product of inertia, slug-ft^2
K_Z	dimensionless radius of gyration about the Z axis, wing spans
K_{p/δ_a}	gain of simplified $\frac{p}{\delta_a}$ transfer function
K_{r/δ_r}	gain of simplified $\frac{r}{\delta_r}$ transfer function
K_{β/δ_r}	gain of simplified $\frac{\beta}{\delta_r}$ transfer function
M	Mach number
S	wing area, sq ft
V	velocity, ft/sec
W	gross weight of airplane, lb
b	wing span, ft

c local chord of the wing measured parallel to the plane of symmetry

c_l section lift coefficient

g acceleration due to gravity, ft/sec^2

m mass of airplane, slugs

m_F effective mass for lateral acceleration of flexible airplane, $m - \frac{q_o S}{V} C_{Y_{\dot{\beta}}}$

n normal acceleration, positive downward, gravity units

p rolling velocity, radians/sec

q_o dynamic pressure, lb/sq ft

r yawing velocity, radians/sec

t time, sec

z structural deflection, positive downward, in.

z_o vertical coordinate, positive downward, in.

α angle of attack, radians

β angle of sideslip, radians (except as otherwise noted)

δ_a total aileron deflection, measured in a plane perpendicular to the hinge line, positive right aileron up, radians (except as otherwise noted)

δ_r rudder deflection, measured in a plane perpendicular to the hinge line, positive trailing edge left, radians (except as otherwise noted)

ζ damping ratio

ζ_a damping ratio of numerator term of $\frac{p}{\delta_a}$ transfer function

η spanwise coordinate, in wing semispans

μ parameter used in evaluating aerodynamic derivatives from transfer-function coefficients, defined in equation (10)

τ rolling-mode time constant, sec

φ angle of bank, radians

$\Phi_{\left(\frac{\text{output}}{\text{input}}\right)}$ phase angle of output quantity minus phase angle of input quantity

ψ angle of yaw, radians

ω frequency, radians/sec

ω_a undamped natural frequency of numerator term of $\frac{p}{\delta_a}$ transfer function

ω_n undamped natural frequency, radians/sec

C_{l_β}, C_{n_β}, C_{l_δ}, C_{n_δ}, $C_{n_{\dot\beta}}$, C_{Y_β}, $C_{Y_{\dot\beta}}$, $C_{Y_{\dot\psi}}$, C_{Y_δ}, C_{Y_φ}, $C_{n_{\dot\psi}}$, $C_{l_{\ddot\varphi}}$, $C_{l_{\ddot\psi}}$, $C_{n_{\ddot\psi}}$ } derivative of coefficient with respect to subscript

C_{l_r}, C_{n_r}, C_{l_p}, C_{n_p} derivative of coefficient with respect to subscript $\times \frac{b}{2V}$

L_p $\frac{q_o S b^2}{2V I_{X_F}} C_{l_p}$, per sec

L_r $\frac{q_o S b^2}{2V I_{X_F}} C_{l_r}$, per sec

L_β $\frac{q_o S b}{I_{X_F}} C_{l_\beta}$, per sec^2

N_p $\frac{q_o S b^2}{2V I_{Z_F}} C_{n_p}$, per sec

N_r $\frac{q_o S b^2}{2V I_{Z_F}} C_{n_r}$, per sec

N_β $\frac{q_o Sb}{I_{Z_F}} C_{n_\beta}$, per sec^2

Y_β $\frac{q_o S}{m_F V} C_{Y_\beta}$, per sec

Y_φ $\frac{g}{V}$, per sec

L_δ $\frac{q_o Sb}{I_{X_F}} C_{l_\delta}$, per sec^2

N_δ $\frac{q_o Sb}{I_{Z_F}} C_{n_\delta}$, per sec^2

Y_δ $\frac{q_o S}{m_F V} C_{Y_\delta}$, per sec

r_{X_F} $\frac{I_{XZ}}{I_{X_F}} + \frac{q_o SbC_{l_{\dot{\psi}}}}{I_{X_F}}$

r_{Z_F} $\frac{I_{XZ}}{I_{Z_F}}$

L_p' $L_p + r_{X_F} N_p$

L_β' $L_\beta + r_{X_F} N_\beta$

N_r' $N_r + r_{Z_F} L_r$

N_β' $N_\beta + r_{Z_F} L_\beta$

L_δ' $L_\delta + r_{X_F} N_\delta$

N_δ' $N_\delta + r_{Z_F} L_\delta$

Subscripts

B	body axis
cg	center of gravity
t	tail
wt	left wing tip

Dots are used to indicate differentiation with respect to time; for example, $\dot{\beta} = \frac{d\beta}{dt}$.

TEST EQUIPMENT

The test airplane was a Boeing B-47A with wing vortex generators installed (fig. 1). An external nose boom and an optigraph for measuring the movements of target lights mounted on the wing and tail were added (figs. 1 and 2). Pertinent physical characteristics are listed in table I. Left and right aileron, and rudder deflections were each measured by three NACA resistance-type control-deflection indicators located at the root, midspan, and tip. An examination of these records indicated that there was a negligible difference in deflections at the root, midspan, and tip of the control surfaces for the flight conditions investigated. Therefore only the midspan deflection records were used in the analysis. Wing accelerations were measured with Statham linear accelerometers. These quantities were recorded on Weston 12-channel and Consolidated 18-channel oscillographs. Self-recording turn meters were used to measure roll and yaw rates at the center of gravity and tail. Sideslip angles were measured with a vane-type pickup. The instruments were aligned with respect to the body reference line and locations of the pertinent instruments are shown in figure 2.

TEST PROCEDURE

Responses to both aileron and rudder pulses were obtained for a Mach number range from 0.6 to 0.82 at an altitude of 35,000 feet. This Mach number range is that in which, from an examination of wind-tunnel data, the aerodynamic derivatives could be expected to be constant for a given flight condition, and thus linear analysis techniques could be used. The center-of-gravity location was approximately 21 percent of the mean aerodynamic chord and the gross weight was approximately 115,000 pounds. The maneuvers consisted of the pilot applying a sharp aileron or rudder pulse with the other controls held fixed, and then allowing the airplane to

oscillate for about 25 seconds (yaw damper off). The transient motion did not completely subside in this time because of the lightly damped Dutch roll mode. Typical time histories are shown in figures 3 and 4. In order to show the structural vibrations more clearly, only the first portion of several of the records is presented. In addition, complete records are shown for roll rate, yaw rate, and sideslip-angle responses to the rudder pulse to illustrate the motion due to the Dutch roll mode. For some of the maneuvers, a small amount of Dutch roll motion was present when the control input was applied. This effect has been subtracted out of the time histories shown in order to indicate more clearly the response to the control-surface motions.

PREDICTED DYNAMIC RESPONSES

The dynamic-response characteristics of the airplane are more easily interpreted if the time histories are converted to frequency-response or transfer-function form. In order to establish the relationships between these forms of the dynamic response, a knowledge of the equations of motion is necessary. These equations also provide a basis for determining approximate relations for transfer-function coefficients and aerodynamic derivatives.

Equations of Motion

In order to define completely the motions of a flexible airplane, a prohibitively large number of degrees of freedom would be needed. Hence, for practical purposes, only the most significant degrees of freedom can be included. A simplification of particular interest from the standpoint of control studies is the use of equations of motion for a rigid airplane with the coefficients modified to include the pseudostatic effects of flexibility. In the pseudostatic method, as discussed in references 1 and 2, the structural deformations are assumed to be in phase with the aerodynamic and inertial loads resulting from airplane motions. The aerodynamic forces arising from these deformations are included by modifying the derivatives in the airplane equations of motion.

Three-degree-of-freedom lateral-directional equations of motion with respect to stability axes are given in Appendix A. For the flexible airplane appropriate derivatives corresponding to structural deflections due to inertial and dead-weight forces resulting from airplane motions have been added to the equations. These additional terms are then combined with the corresponding rigid airplane inertias to form an effective inertia for the flexible airplane. As explained in Appendix A, it was found to be permissible to neglect a number of the inertial derivatives since the cumulative effect of these quantities on the transfer-function coefficients was found to be negligible.

Aerodynamic Derivatives

The stability derivatives were obtained by available theory and wind-tunnel data. Effects of structural deflections on the derivatives were obtained through use of aerodynamic and structural influence coefficients in the manner described in reference 1. The chordwise centers of pressure of all aerodynamic loads, except loads due to the rudder and ailerons, were assumed to be at the quarter-chord line of their respective surfaces. The average chordwise center of pressure for loads due to the rudder was estimated to be the 0.48 chord from the pressure-distribution data given in reference 5. Although no pressure-distribution data were available for the specific wing-aileron plan form, the center of pressure for the aileron loads was estimated to be at the 0.58 chord from an examination of pressure distributions on similar swept-wing plan forms. Fuselage influence coefficients used in the analysis were obtained from data given in references 6 and 7 and are listed in table II together with the wing influence coefficients which were obtained from reference 8. Wing stations and equivalent weights used in the analysis are shown in figure 5. An example of the application of the method to obtain the effect of wing deflections on the derivative C_{l_β} is given in Appendix B. Predicted aerodynamic derivatives for both the flexible and rigid conditions are listed in table III.

Transfer-Function Coefficients

Transfer functions obtained by solving the three-degree-of-freedom equations are presented in Appendix A. As noted in this Appendix, some of the transfer functions may be simplified for the frequency range of interest. After the spiral mode is neglected, rolling response to aileron becomes

$$\frac{p}{\delta_a} = \frac{A_3(D^2 + a_1 D + a_2)}{(D + D_r)(D^2 + c_1 D + c_2)} \tag{1}$$

The transfer function may also be written as

$$\frac{p}{\delta_a} = \frac{K_{p/\delta_a}[1 + 2\zeta_a D/\omega_a + (D/\omega_a)^2]}{(1 + \tau D)[1 + 2\zeta D/\omega_n + (D/\omega_n)^2]} \tag{2}$$

For yawing and sideslipping response to rudder motion, both spiral and rolling modes may be neglected so that

$$\frac{r}{\delta_r} = \frac{H_r D}{D^2 + c_1 D + c_2} \tag{3}$$

$$\frac{\beta}{\delta_r} = \frac{J_\beta}{D^2 + c_1 D + c_2} \tag{4}$$

These quantities may also be expressed as

$$\frac{r}{\delta_r} = \frac{K_r/\delta_r D}{1 + 2\zeta D/\omega_n + (D/\omega_n)^2} \tag{5}$$

$$\frac{\beta}{\delta_r} = \frac{K_\beta/\delta_r}{1 + 2\zeta D/\omega_n + (D/\omega_n)^2} \tag{6}$$

The predicted frequency responses may be obtained from the transfer functions after $i\omega$ is substituted for the operator D. The conversion of numerator transfer-function coefficients from stability to body axes for comparison with frequency responses measured with respect to body axes is given in Appendix A.

Approximate Equations to Obtain Aerodynamic Derivatives From Transfer-Function Coefficients

The equations for the aerodynamic derivatives were obtained as follows: The coefficients C_3, C_2, and C_1 of the characteristic equation given in Appendix A were expressed in terms of their principal aerodynamic derivatives. The coefficients were also expressed in terms of the factors of the characteristic equation D_r, c_1, and c_2. By equating the coefficients of like powers of D, three simultaneous equations were obtained with three unknowns, L_p, $N_r + Y_\beta$, and N_β'. A cubic equation for L_p was then obtained by eliminating the other unknowns. The derivative L_p was found by using an approximate solution for a cubic equation together with an approximate equation for the amplitude of the roll to yaw ratio of the Dutch roll mode, $\left|\frac{p}{r}\right|$. Equations for the two other derivatives could then be obtained. The equations are

$$L_p = -D_r - \mu \tag{7}$$

$$N_r + Y_\beta = \mu - c_1 \tag{8}$$

$$N_\beta' = c_2 + \mu(D_r - c_1) \tag{9}$$

where

$$\mu = \frac{\left|\frac{p}{r}\right|(N_p - Y_\varphi - D_r r_Z)}{\sqrt{1 + D_r^2/c_2}} \tag{10}$$

Note that these equations correspond to those given in reference 4 except for the quantity μ. The additional term μ could be considered as a measure of the coupling between the Dutch roll and rolling modes. The equation used for L_β' was obtained from reference 4

$$L_\beta' = \left|\frac{p}{r}\right| N_\beta' \sqrt{1 + L_p^2/c_2} \tag{11}$$

Approximate relations for control effectiveness were obtained by substituting typical numerical values in the equations given in Appendix A, and the following expressions (analogous to those given in ref. 4) were found to be valid for the present airplane. The rudder effectiveness derivative was obtained from

$$N_{\delta_r} = H_r \quad \text{or} \quad -J_\beta \tag{12}$$

while aileron effectiveness was obtained from

$$L_{\delta_a} = A_3 \tag{13}$$

Aerodynamic derivatives may be found from the quantities on the left-hand side of equations (7) through (13) through use of the definitions given in the notation.

Thus the aerodynamic derivatives may be obtained from transfer-function coefficients matched from experimental data, provided that an estimate is made of the product of inertia, the derivative C_{n_p}, and also the effective moments of inertia for the flexible airplane. Estimated variations in effective inertia characteristics are presented in figure 6. The principal effect of flexibility is to reduce the rolling moment of inertia. This effect is largely due to the mass of the wing-mounted

nacelles. In order to demonstrate the adequacy of the approximate equations, predicted transfer-function coefficients were first calculated from the predicted derivatives (table III) using the complete expressions for the transfer-function coefficients. Then approximate values of the derivatives were calculated from the predicted transfer-function coefficients using equations (7) to (11), and also using the equations with $\mu = 0$, which correspond to the equations given in reference 4. Comparisons of these derivatives are shown in figure 7. Also shown are derivatives calculated from equations given in reference 4. In all cases the values of derivatives using the approximate equations are closer to the estimated values than those obtained using the equations from reference 4. This is particularly true for the derivative, $C_{n_r} + 2K_Z^2 C_{Y_\beta}$. Although not shown, a similar comparison was made for the rigid case, and the inclusion of the quantity μ also improved the agreement with the predicted derivatives.

REDUCTION OF EXPERIMENTAL DATA

Frequency Response

The Fourier integral was used to convert the transient responses to frequency-response form. The calculation of the Fourier integral consisted first of a numerical integration over the first part of the record using a parabolic fit of the time history similar to that described in reference 9. For the control inputs the time histories showed a constant value after a certain time and hence the remaining portion of the integral was evaluated using an analytical expression for the small step displacement. The response time histories did not reach a constant value since the Dutch roll oscillation was very lightly damped, and analytical expressions for both a step and a damped sinusoidal oscillation (e.g., ref. 10) were used to evaluate the remaining part of the integrals. These calculations were performed on a card-programmed IBM 650 digital computer.

All traces were read at 0.05-second intervals except sideslip angle, which was read at 0.1-second intervals. In some cases, Fourier transforms were obtained from roll and yaw angular-acceleration traces in order to define better the corresponding angular rate traces at higher frequencies. Results from sideslip records at the higher frequencies are not presented because of the lack of well-defined trends. This is probably due to the relative attenuation of the higher frequency amplitudes measured by an angular displacement instrument as compared with those measured by angular rate instruments. Phase-angle corrections were made for the dynamic response of the instruments.

Transfer-Function Coefficients and Aerodynamic Derivatives

Transfer-function coefficients of the simplified transfer functions for p/δ_a, r/δ_r, and β/δ_r described in a previous section were obtained by matching the response time histories (e.g., figs. 3 and 4) by means of an analog computer. They were then converted from body axes to stability axes. In some cases, small residual oscillations, which were principally due to the lightly damped Dutch roll mode, were present when the airplane control pulse was applied. Initial conditions were applied to the simulator to include this motion, although in all cases this had only a small effect on transfer-function coefficients. In matching the time histories of p/δ_a on the analog computer, it was found convenient to represent the third-order transfer function by parallel networks of first-order and second-order transfer functions. This representation is equivalent to separating the third-order transfer function into the partial fraction form shown in Appendix A. In this way contributions of the Dutch roll and rolling modes to the resultant motions could be matched separately.

Aerodynamic derivatives were then obtained from the appropriate transfer-function coefficients using the approximate equations (eqs. (7) to (13)) given in the previous section.

RESULTS AND DISCUSSION

Frequency Responses

In the discussion that follows, effects of the relatively low frequency lateral-directional modes will be investigated first. Comparisons will be made between measured and predicted responses to determine the frequency range for which the predictions are adequate. Then the higher frequency structural modes will be discussed and compared with values obtained from the ground oscillation tests of reference 11. The frequency-response data to be presented include: measured frequency responses to aileron and rudder inputs over a fairly wide Mach number range (figs. 8 and 9), typical comparisons of measured responses at the center of gravity and tail (figs. 10 and 11), and typical comparisons of measured and estimated frequency responses (figs. 12 and 13).

Lateral-directional modes.- The ailerons excite principally the rolling mode as well as some Dutch roll mode as shown in the roll-rate response (fig. 8(a)), which is seen to be of the same form as that indicated in equation (2). The rolling mode (a first-order term) causes the net shift of 90° in the phase angle between the frequencies of 0.5 to 5 radians per second and the slope of the amplitude curve in the frequency range of 2 to 7 radians per second, while the peak in the amplitude curve

that occurs at frequencies from about 1 to 1.5 radians per second is due to the Dutch roll mode (a second-order term). Responses in sideslip and yaw rate are quite small (figs. 8(b) and 8(c)). The rudder mainly excites the Dutch roll mode (fig. 9). For both inputs, differences in tail and center-of-gravity roll and yaw rates are small in this frequency range. This may also be seen from the time histories (figs. 3 and 4).

The predicted results for the flexible airplane in general agree reasonably well with experimental results for frequencies up to about 3 to 8 radians per second, with the possible exception of wing-tip acceleration (figs. 12(e) and 13(f)). Also some discrepancies are apparent in the lowest frequency range (near 0.5 radian/sec) which is the region in which the experimental frequency-response accuracy obtained from pulse-type inputs becomes relatively poor, as was discussed in references 1 and 4. For the aileron responses, the predicted gain for the flexible case is much lower than that for the rigid, reflecting the reduction in aileron effectiveness. However, the p/δ_r responses (fig. 13(a)) indicate a higher gain for the flexible case. This is largely due to the higher value of the ratio of C_{l_β} to the effective moment of inertia in the flexible case. Flexibility also reduces the frequency and damping of the Dutch roll mode. A discrepancy between theory and experiment in the curves for r/δ_a (fig. 12(b)) is that the experimental phase angles shift 180° while the predicted values approach a 360° shift. One possible explanation is that the smaller phase shift could have been obtained from the predicted curve if a more negative value of $C_{n_{\delta_a}}$ had been assumed. A structural mode could also affect the phase angle in this region.

Structural modes.- A peak occurs in all the frequency responses to aileron (fig. 8) at about 13.4 radians per second which will be called the first wing antisymmetric bending mode. This compares with 14.4 radians per second obtained from ground vibration tests (ref. 11). The mode is particularly noticeable in the center-of-gravity roll rate and wing-tip acceleration responses. In the time history for the wing optigraph, this mode is seen to predominate. Another point of interest is that the amplitude of the yaw rate at the tail is greater than that for the center of gravity, as may be seen from both the frequency-response and time-history curves. The mode frequency remains essentially constant for the flight range investigated although there is a slight increase in amplitude with Mach number. Measurements of the time history indicated that the damping was also essentially constant over the flight range at a value of about 0.025 critical.

The shape of this mode, obtained from measurements of the free oscillation amplitudes of the accelerometer and turn-meter traces resulting from aileron inputs, is shown in figure 14. When the curve was determined, small corrections for chordwise displacement of the instruments were made where necessary to transfer the accelerometer results to the 17-percent and 58-percent chord lines corresponding to the front and rear

spars, respectively. In the placement of pickups for an autopilot system, it is desirable to locate them at points on the structure that are least affected by the structural modes in order to avoid introducing undesired signals. For a roll gyro, the optimum location for minimizing the angular velocity input of the antisymmetric wing mode would be where the wing mode shape has zero slope which, as shown in figure 14, is at $\eta = 0.38$ near the inboard nacelle, while for a linear accelerometer, the optimum location would be at a nodal point, which in figure 14 is at η of about 0.55 just outboard of the nacelle. The wing accelerometer node line obtained from the two span positions shows good agreement with that obtained from ground vibration tests.

In the wing-tip acceleration curve (fig. 8(d)), a dip in the amplitude and a shift of approximately 180° in the phase angle relative to the center-of-gravity roll rate (fig. 8(a)) occurs in a frequency range somewhat lower than the wing bending frequency. This motion can be illustrated as follows: At low frequencies, the relation between wing bending and roll angle is as shown in sketch (a). As the frequency increases, the amount of

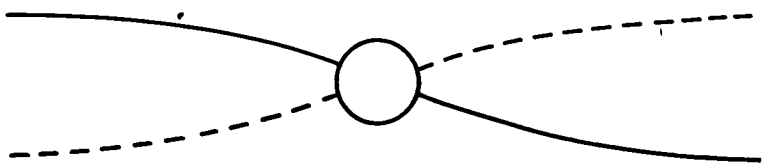

Sketch (a)

wing bending relative to roll angle becomes greater so that the acceleration at the tip reverses sign with respect to the roll angle (sketch (b)).

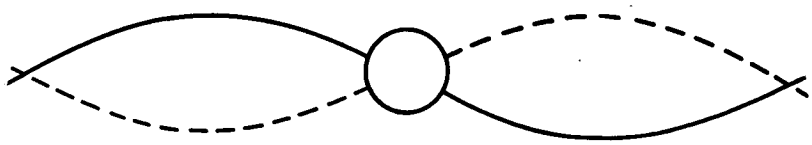

Sketch (b)

This trend continues until the bending frequency is reached.

An examination of figure 8 shows that no additional modes were excited to any appreciable extent in the measured frequency range above that of the wing first antisymmetric bending mode, although two modes were measured from ground vibration tests (ref. 11).

While the rudder pulses also excite the wing antisymmetric bending mode, their principal effect is to excite two slightly higher frequency modes which are predominantly fuselage modes as may be seen from the

responses of yaw and roll rate at the tail and center of gravity (figs. 9 and 11). The lower frequency, which is predominantly fuselage side bending, is 16.5 radians per second while the upper frequency, which is principally fuselage torsion, is 23 radians per second. These frequencies compare with ground vibration test values of 18.0 and 24.5 radians per second, respectively (ref. 11). The prominance of these modes at the tail may also be seen from the transient responses due to the rudder input (fig. 4).

The frequency responses for roll and yaw rate at the tail due to a rudder pulse (fig. 11) also indicate regions of low amplitude at frequencies below the structural natural frequencies (about 3 to 8 radians per second). While phase angle for the tail yaw rate shifts 180° out of phase with that of the center of gravity, as was the case for the wing at frequencies below that of the antisymmetric bending mode, the phase angle shifts for the tail and center-of-gravity roll rate are approximately the same so that they remain in phase. It is of interest to note that by the inclusion of only the pseudostatic effects of sideslip, yawing acceleration, etc., on the tail deflections, these amplitude and phase-angle trends are predicted (figs. 13(b) and 13(d)). While the direction of the 180° phase-angle shift does not agree for the tail yaw rate, the resultant shift is the same. Since the amplitude ratio is quite low in this region, some question does exist as to the direction of the phase-angle shifts for both the experimental and predicted values.

Transfer-Function Coefficients

Comparisons of experimentally determined transfer-function coefficients with predicted values (with respect to stability axes) for both the flexible and rigid case based on the simplified transfer functions (eqs. (2), (5), and (6)) are shown in figure 15. In general, agreement between experiment and theory for both numerator and denominator is seen to be good, as was the case reported in reference 2 for 25,000 feet.

For the denominator terms, the values of measured damping ratio are an average of 0.015 less than the estimated flexible values. While the ratios of measured to estimated values are relatively large, the average magnitude is approaching zero at the lower values of Mach number, and hence the discrepancy is considered to be small. Also some scatter occurred in the time constant τ. This parameter was difficult to evaluate because it did not have as important an effect on the transient response to a pulse as did the other parameters. Flexibility is seen to reduce both the frequency and damping of the Dutch roll mode. These reductions are caused primarily by the decrease in vertical-tail effectiveness due to fuselage and tail flexibility having a larger effect than the decrease in effective yawing moment of inertia. Flexibility changes the time constant τ very little. This term depends principally on the

ratio of effective rolling moment of inertia to the aerodynamic damping in roll. Since the rolling moment of inertia is due largely to the nacelle and wing weights, wing flexibility reduces both the aerodynamic and inertia loads by about the same amount.

For the numerator terms also, good agreement is obtained between theory and experiment. The scatter that occurred in the measured values of ζ_a resulted from the small effect of ζ_a on the time histories matched with the analog computer. The comparison of the matched curves in figures 3 and 4 with the measured time histories indicates that the transfer functions corresponding to the Dutch roll mode only for the rudder pulses, and the rolling and Dutch roll modes for the aileron pulses were sufficient to define the time histories adequately. The greatest effect of flexibility is seen to be in the reduction in gain for p/δ_a. This reflects the reduction in aileron effectiveness associated with outboard ailerons. The predicted values of ζ_a and ω_a are slightly different from ζ and ω_n and approach these quantities at the higher Mach numbers. These differences depend upon the aerodynamic derivatives that effect the quantities μ and $C_{n_{\delta_a}}$, which become relatively small at the higher Mach numbers and corresponding low angles of attack. These effects are reflected in the time histories by the amount of excitation of the Dutch roll mode and also by a reduction in over-all gain. For the limiting case of $\zeta_a = \zeta$ and $\omega_a = \omega_n$, effects of the Dutch roll mode are eliminated and the transfer function (eq. (2)) reduces to a first-order form.

Aerodynamic Derivatives

Generally good agreement is obtained between predicted and experimental values of the aerodynamic derivatives (fig. 16). Differences between predicted aerodynamic derivatives for the flexible and rigid cases are generally somewhat greater than the differences between transfer-function coefficients since the latter are partially compensated by changes in the effective moments of inertia due to flexibility. In general, flexibility tends to reduce the values of the aerodynamic derivatives with the largest reduction occurring for $C_{l_{\delta_a}}$ and C_{l_p}. However, flexibility tends to increase the magnitude of C_{l_β} since the usual decrease in value of a derivative due to flexibility is more than compensated by the increase in dihedral due to wing lift.

CONCLUSIONS

The dynamic lateral-directional responses to aileron and rudder pulses of a large flexible airplane for flight conditions of 0.6 to 0.82 Mach number and an altitude of 35,000 feet have been investigated and compared with

predicted responses based on the lateral-directional equations of motion. Pseudostatic effects of flexibility were included through use of structural and aerodynamic influence coefficients. The following conclusions have been made:

1. The manually applied pulse technique was found to be adequate to obtain data suitable for defining frequency responses for the frequency range from 1 to 25 radians per second. This range includes the relatively low frequency Dutch roll and rolling modes, as well as the higher frequency wing first antisymmetric bending, fuselage side-bending, and fuselage torsion modes.

2. Reasonably good agreement was obtained in the frequency range below about one half of the lowest structural frequency between measured and estimated frequency responses.

3. The principal effect of flexibility on predicted transfer-function coefficients is the reduction in gain of airplane response to aileron motion, reflecting the reduction in aileron effectiveness, and also a reduction in damping and frequency of the Dutch roll mode.

4. The principal lateral-directional derivatives and control-effectiveness derivatives, which were evaluated from measured transfer functions through use of approximate equations, indicated good agreement, in general, with predicted derivatives when the pseudostatic effects of flexibility were included.

5. In the frequency range above half the lowest structural frequency, the effects of structural modes were sufficiently large (even at the center of gravity) for the responses measured, so that predictions of the frequency responses, which included only the pseudostatic effects of flexibility, were inadequate.

6. The frequencies of the three structural modes measured in flight were within about 10 percent of the frequencies of the corresponding modes measured in ground vibration tests. In addition, the wing node line for the wing first antisymmetric bending mode measured in flight showed good agreement with that obtained from the ground vibration test.

Ames Aeronautical Laboratory
National Advisory Committee for Aeronautics
Moffett Field, Calif., Oct. 8, 1956

APPENDIX A

PREDICTED AIRPLANE RESPONSE

Equations of Motion

The three lateral-directional equations of motion with respect to stability axes given in Appendix C of reference 4 for a rigid airplane will be modified for use for a flexible airplane. For the flexible case, additional terms must be added to take account of aerodynamic forces resulting from structural deflections due to inertial loads ($C_{l_{\ddot{\varphi}}}$, $C_{l_{\ddot{\psi}}}$, $C_{n_{\ddot{\psi}}}$, $C_{Y_{\dot{\psi}}}$, and $C_{Y_{\dot{\beta}}}$) and dead-weight loads ($C_{Y_{\varphi}}$). A more complete evaluation of these additional derivatives would also have included other derivatives dependent on $\ddot{\varphi}$, $\ddot{\psi}$, $\dot{\psi}+\dot{\beta}$, and φ. However, by the substitution of typical numerical values in the transfer-function coefficients, the cumulative effects of these other derivatives on the transfer-function coefficients were found to be negligible even though some of them were of appreciable size (e.g., $C_{n_{\dot{\psi}}}$ and $C_{n_{\dot{\beta}}}$ were several times larger than $C_{n_r}(b/2V)$ for the largest values of M). The rolling moment, yawing moment, and side-force equations, with flight-path angle assumed zero, may be expressed as

$$\left(I_X D^2 - q_o SbC_{l_{\ddot{\varphi}}} D^2 - q_o SbC_{l_p} \frac{b}{2V} D\right)\varphi +$$

$$\left(-I_{XZ} D^2 - q_o SbC_{l_{\ddot{\psi}}} D^2 - q_o SbC_{l_r} \frac{b}{2V} D\right)\psi - q_o SbC_{l_\beta}\beta = q_o SbC_{l_\delta}\delta \qquad (A1)$$

$$\left(-I_{XZ} D^2 - q_o SbC_{n_p} \frac{b}{2V} D\right)\varphi +$$

$$\left(I_Z D^2 - q_o SbC_{n_{\ddot{\psi}}} D^2 - q_o SbC_{n_r} \frac{b}{2V} D\right)\psi - q_o SbC_{n_\beta}\beta = q_o SbC_{n_\delta}\delta \qquad (A2)$$

$$\left(-W - q_o SC_{Y_\varphi}\right)\varphi + \left(mVD - q_o SC_{Y_{\dot{\psi}}} D\right)\psi + \left(mVD - q_o SC_{Y_{\dot{\beta}}} D - q_o SC_{Y_\beta}\right)\beta = q_o SC_{Y_\delta}\delta \qquad (A3)$$

The remaining inertial deflection derivatives were then combined with the mass terms to form effective inertias for the flexible airplane. Thus

$$I_{X_F} = I_X - q_o S b C_{l_{\ddot{\varphi}}}$$

$$I_{Z_F} = I_Z - q_o S b C_{n_{\ddot{\psi}}}$$

$$m_F = m - \frac{q_o S}{V} C_{Y_{\dot{\beta}}}$$

$$\text{or } m - \frac{q_o S}{V} C_{Y_{\dot{\psi}}}$$

Since the derivatives $C_{Y_{\dot{\psi}}}$ and $C_{Y_{\dot{\beta}}}$ each represent aerodynamic forces due to lateral acceleration, they are of equal magnitude, and hence m_F may be expressed in terms of either derivative. The three equations (A1), (A2), and (A3) can then be written in a more convenient form by dividing them by I_{X_F}, I_{Z_F}, and $m_F V$, respectively, and introducing new symbols

$$\left(D^2 - L_p D\right)\varphi + \left(-r_{X_F} D^2 - L_r D\right)\psi - L_\beta \beta = L_\delta \delta \tag{A4}$$

$$\left(-r_{Z_F} D^2 - N_p D\right)\varphi + \left(D^2 - N_r D\right)\psi - N_\beta \beta = N_\delta \delta \tag{A5}$$

$$-Y_\varphi \varphi + D\psi + (D - Y_\beta)\beta = Y_\delta \delta \tag{A6}$$

Note that the term Y_φ (which equals g/V) remains the same as for the rigid case since the derivative C_{Y_φ} is due to dead-weight loads that are distributed in the same manner as the lateral acceleration loads.

Transfer Functions

Transfer-function coefficients for φ/δ, ψ/δ, and β/δ can be obtained by simultaneous solution of the three equations (A4), (A5), and (A6).

Denominator coefficients.- The denominator of the transfer functions, Δ, may be expressed as

$$\Delta = D(C_4D^4 + C_3D^3 + C_2D^2 + C_1D + C_0)$$

where

$$C_4 = 1 - r_{X_F}r_{Z_F}$$

$$C_3 = -L_p' - N_r' - Y_\beta\left(1 - r_{X_F}r_{Z_F}\right)$$

$$C_2 = N_\beta' + Y_\beta(L_p' + N_r') + L_pN_r - N_pL_r$$

$$C_1 = L_\beta N_p - N_\beta L_p - Y_\varphi L_\beta' + Y_\beta(L_rN_p - N_rL_p)$$

$$C_0 = Y_\varphi(L_\beta N_r - N_\beta L_r)$$

For the moderate angle-of-attack range considered, r_{X_F} and r_{Z_F} are small quantities and hence $C_4 \approx 1$. The denominator can then be expressed in factored form as

$$\Delta = D(D + D_s)(D + D_r)(D^2 + c_1D + c_2)$$

where D_s and D_r represent the spiral and rolling modes, respectively, and c_1 and c_2 are coefficients that define the damping and frequency of the Dutch roll mode.

Numerator coefficients.- With $p = D\varphi$, and $r = D\psi$, the numerator coefficients of the following transfer functions can be expressed in terms of the derivatives.

$$\frac{p}{\delta} = \frac{D(A_3D^3 + A_2D^2 + A_1D)}{\Delta}$$

where

$$A_3 = L_\delta'$$

$$A_2 = -Y_\beta L_\delta' + N_\delta L_r - L_\delta N_r + Y_\delta L_\beta'$$

$$A_1 = L_\delta N_\beta - N_\delta L_\beta + Y_\beta(L_\delta N_r - N_\delta L_r) + Y_\delta(L_rN_\beta - N_rL_\beta)$$

$$\frac{r}{\delta} = \frac{D(B_3D^3 + B_2D^2 + B_1D + B_0)}{\Delta}$$

where

$$B_3 = N_{\delta}'$$

$$B_2 = L_{\delta}N_p - N_{\delta}L_p - Y_{\beta}N_{\delta}' + Y_{\delta}N_{\beta}'$$

$$B_1 = Y_{\beta}(N_{\delta}L_p - L_{\delta}N_p) + Y_{\delta}(L_{\beta}N_p - N_{\beta}L_p)$$

$$B_0 = Y_{\varphi}(L_{\delta}N_{\beta} - N_{\delta}L_{\beta})$$

$$\frac{\beta}{\delta} = \frac{D(E_3D^3 + E_2D^2 + E_1D + E_0)}{\Delta}$$

where

$$E_3 = Y_{\delta}\left(1 - r_{X_F}r_{Z_F}\right)$$

$$E_2 = -Y_{\delta}(N_r' + L_p') - N_{\delta}'$$

$$E_1 = Y_{\varphi}L_{\delta}' + N_{\delta}L_p - L_{\delta}N_p + Y_{\delta}(L_pN_r - N_pL_r)$$

$$E_0 = Y_{\varphi}(N_{\delta}L_r - L_{\delta}N_r)$$

Simplifications of the transfer functions.- When transfer functions are evaluated from measured data, it is desirable to use as simple a form as possible which will still adequately fit the data. Calculations indicated that the spiral mode factor D_s was very small and could be neglected for the frequency range of interest. Thus the rolling response to aileron was simplified to

$$\frac{p}{\delta_a} = \frac{A_3(D^2 + a_1D + a_2)}{(D + D_r)(D^2 + c_1D + c_2)}$$

where

$$a_1 = \frac{A_2}{A_3}$$

$$a_2 = \frac{A_1}{A_3}$$

To determine estimated values for use with the curve fitting of the measured responses on the analog computer, a partial fraction form of the transfer function was advantageous to use.

$$\frac{p}{\delta_a} = \frac{G_p}{D + D_r} + \frac{H_p D + J}{D^2 + c_1 D + c_2}$$

In obtaining approximate relations for r/δ_r and β/δ_r, it was desirable first to write the transfer functions in partial fraction form.

$$\frac{r}{\delta_r} = \frac{F_r}{D + D_s} + \frac{G_r}{D + D_r} + \frac{H_r D + J_r}{D^2 + c_1 D + c_2}$$

$$\frac{\beta}{\delta_r} = \frac{F_\beta}{D + D_s} + \frac{G_\beta}{D + D_r} + \frac{H_\beta D + J_\beta}{D^2 + c_1 D + c_2}$$

By the substitution of typical numerical values, all numerator terms were found to be negligible except H_r and J_β. Thus, the transfer-function coefficients could be simplified to

$$\frac{r}{\delta_r} = \frac{H_r D}{D^2 + c_1 D + c_2}$$

$$\frac{\beta}{\delta_r} = \frac{J_\beta}{D^2 + c_1 D + c_2}$$

Transfer functions for the rear part of the fuselage and the wing tip.- In addition to the transfer-function coefficients for quantities at the center of gravity, the coefficients for r_t/δ, p_t/δ, and n_{wt}/δ are needed. The evaluation of these quantities includes responses at the center of gravity and also responses due to pseudostatic structural deflections at the particular location. The equation for yaw rate at the rear part of the fuselage is

$$\frac{r_t}{\delta} = \frac{r}{\delta} + \frac{D\Delta\psi_t}{\delta}$$

where $\Delta\psi_t$ represents the total change in angle of yaw in radians at the rear part of the fuselage due to structural deformations resulting from a control input. The following quantities were included in determining $\Delta\psi_t/\delta$

$$\frac{\Delta\psi_t}{\delta} = \frac{\Delta\psi_t}{\beta}\frac{\beta}{\delta} + \frac{\Delta\psi_t}{r}\frac{r}{\delta} + \frac{\Delta\psi_t}{\ddot{\psi}}\frac{\ddot{\psi}}{\delta} + \frac{\Delta\psi_t}{\delta}$$

For instance $\Delta\psi_t/\beta$ represents the pseudostatic change in angle of yaw at the rear part of the fuselage due to structural deformations resulting from a unit change in β.

Similarly, the equation for roll rate at the rear part of the fuselage is

$$\frac{p_t}{\delta} = \frac{p}{\delta} + \frac{D\Delta\varphi_t}{\delta}$$

where $\Delta\varphi_t$ represents the total change in angle of roll at the rear part of the fuselage due to structural deformations resulting from a control input and may be expressed as

$$\frac{\Delta\varphi_t}{\delta} = \frac{\Delta\varphi_t}{\beta}\frac{\beta}{\delta} + \frac{\Delta\varphi_t}{r}\frac{r}{\delta} + \frac{\Delta\varphi_t}{\ddot{\psi}}\frac{\ddot{\psi}}{\delta} + \frac{\Delta\varphi_t}{\delta}$$

The equation for acceleration at the left wing tip is

$$\frac{n_{wt}}{\delta} = -\frac{Dp}{\delta} + \frac{D^2 z_{wt}}{12\delta}$$

Calculations indicated that the effect of $D^2 z_{wt}/\delta$ was small for the frequency range up to the first antisymmetric bending frequency and, hence, was neglected.

Conversion of transfer-function coefficients from stability axes to body axes.- In order to compare predicted results with measured frequency responses which were obtained with respect to body axes, the predicted transfer functions were converted from stability-axis to body-axis form. Since, for the angle-of-attack range considered, the quantity C_4 was essentially unity, only the numerator terms of the transfer function need be modified. The equations for conversion from stability axes to body axes are (e.g., ref. 4)

$$p_B = p \cos \alpha - r \sin \alpha$$

$$r_B = r \cos \alpha + p \sin \alpha$$

$$\tan \beta_B = \frac{\tan \beta}{\cos \alpha}$$

For small angles of attack, the equations may be simplified to

$$p_B = p - r\alpha$$

$$r_B = r + p\alpha$$

$$\beta_B = \beta$$

These relations will also hold for derivatives of the angles. Hence, the numerator coefficients for p/δ and r/δ may be converted as follows:

$$A_{i_B} = A_i - B_i\alpha$$

$$B_{i_B} = B_i + A_i\alpha$$

APPENDIX B

EXAMPLE CALCULATION OF WING CONTRIBUTION TO C_{l_β} USING AERODYNAMIC AND STRUCTURAL INFLUENCE COEFFICIENTS

A general description of the method used as applied to symmetrical loadings was given in reference 1. An example application to obtain antisymmetric loadings will be presented here. The equations to be used will be given first, and then a numerical example to obtain C_{l_β} will be shown.

The rolling-moment coefficient resulting from an arbitrary antisymmetric angle-of-attack distribution may be expressed as a power series of the dynamic pressure q.

$$C_{l_F} = C_{l_R} + C_{l_A}q + C_{l_B}q^2 + C_{l_C}q^3 + \cdots \tag{B1}$$

where

C_{l_F} rolling-moment coefficient for the flexible wing

C_{l_R} rolling-moment coefficient for the rigid wing

$C_{l_A}q$ increment in rolling-moment coefficient resulting from structural deflections due to the C_{l_R} loading

$C_{l_B}q^2$ increment in rolling-moment coefficient resulting from structural deflections due to the C_{l_A} loading

For the wing structure considered in the present example, the ratios of all terms after the first one, $-C_{l_A}/C_{l_B}$, $-C_{l_B}/C_{l_C}$, etc., are essentially equal to a single constant k. This result may be interpreted to mean that the successive wing-deflection shapes that produce these loads are essentially the same, and, hence, this portion of the wing loading may be represented as a single-degree-of-freedom system. Thus the incremental rolling-moment coefficient due to this portion of the wing deflections may be represented by the expression $C_{l_A}q/1+kq$ and it will be valid for large positive values of the quantity kq even though the series would not converge for positive kq greater than 1. The equation for rolling-moment coefficient for the flexible wing will then be

$$C_{l_F} = C_{l_R}\left[1 + \frac{q(C_{l_A}/C_{l_R})}{1 + kq}\right] \tag{B2}$$

The quantities in equation (B2) will now be determined through use of aerodynamic and structural influence coefficients.

Antisymmetric aerodynamic influence coefficients were obtained through use of reference 12. First, $p_{\nu n}$ angle-of-attack influence coefficients, which represent the angle of attack at station ν due to a continuous loading function having a unit value at station n and zero value at the other stations, were obtained from reference 12. These were then converted to loading influence coefficients $A_{\nu n}$ (i.e., the loading $c_l c/2b$, at station, n, due to a continuous angle-of-attack distribution with a unit value at station ν and zero values at the other stations) by solving for the span loadings for a unit angle of attack at one control station. This was done for each of the spanwise control stations 1, 2, and 3 located at $\eta = 0.924$, 0.707, and 0.383, respectively. The resulting rolling-moment coefficient for a unit angle of attack at a control station, ν, can then be calculated using the following equation, which has the form of equation 15 in reference 12.

$$C_{l_\nu} = \frac{\pi A}{16}\left[A_{\nu 2} + 0.707(A_{\nu 1} + A_{\nu 3})\right] \tag{B3}$$

The wing structural influence coefficients are listed in table II. For use with the aerodynamic influence coefficients, they were converted to the form of a change in streamwise angle of attack in radians, due to a 1000-pound load at a given percent chord position. All aerodynamic loads were assumed to act along the quarter-chord line except for loads due to the ailerons. The change in streamwise angle of attack at station m due to the loading resulting from an angle of attack at station ν, with $q = 1$ psi, may be expressed as

$$(\epsilon_o)_{\nu m} = \frac{b^2(12)^2}{1000}\sum_{n=1}^{3} A_{\nu n} S_{mn} I_n \tag{B4}$$

with

$$m = 1, 2, 3$$

$$\nu = 1, 2, 3$$

where

$A_{\nu n}$ aerodynamic influence coefficients for the loading function at station n due to an angle of attack at station ν

S_{mn} structural influence coefficients expressing the change in angle of attack at station m in radians due to a 1000-pound load at the quarter-chord station n

I_n integrating factors with the following values

$$I_1 = 0.1502$$

$$I_2 = 0.2776$$

$$I_3 = 0.3628$$

The aerodynamic loading due to $(\epsilon_o)_{\nu m}$ is then obtained from the summation

$$(A_A)_{\nu n} = \sum_{m=1}^{3} (\epsilon_o)_{\nu m} A_{mn} \tag{B5}$$

from which the incremental rolling-moment coefficient may be obtained.

$$\left(C_{l_A}\right)_\nu = \frac{\pi A}{16}\left\{(A_A)_{\nu 2} + 0.707\left[(A_A)_{\nu 1} + (A_A)_{\nu 3}\right]\right\} \tag{B6}$$

The next incremental rolling-moment coefficient $\left(C_{l_B}\right)_\nu$ due to deflection resulting from the loading coefficients $(A_A)_{\nu n}$ is calculated in a similar manner.

Thus, the rolling-moment coefficients resulting from the initial angle of attack, and from the first and second twist distributions can be calculated from the following equations

$$C_{l_R} = \sum_{\nu=1}^{3} C_{l_\nu} \alpha_\nu \tag{B7}$$

$$C_{l_A} = \sum_{\nu=1}^{3} \left(C_{l_A}\right)_\nu \alpha_\nu \tag{B8}$$

$$C_{l_B} = \sum_{\nu=1}^{3} \left(C_{l_B}\right)_\nu \alpha_\nu \tag{B9}$$

The rolling-moment coefficient for the flexible wing for any desired angle-of-attack distribution, α_ν, is then obtained by substituting values from the above equations into equation (B2). The reference rolling-moment coefficients with the aerodynamic loads at the quarter chord were calculated through use of the previous equations (with $q = 1$ psi) and are tabulated in the following table:

ν	1	2	3
C_{l_ν}	0.120	0.298	0.326
$C_{l_{A_\nu}}$	-.0376	-.0698	-.0376
$C_{l_{B_\nu}}$	.00856	.01553	.00796

In order to determine the rolling-moment coefficient for a specific derivative, the wing angle-of-attack distribution must be known. For a unit sideslip angle, the wing contribution to C_{l_β} may be separated into loadings due to two angle-of-attack distributions (ref. 13): (1) a constant spanwise angle-of-attack distribution due to the difference in effective velocity acting on each wing panel for the yawed attitude and (2) an angle-of-attack distribution proportional to the wing dihedral angle, which for this case may be considered to be due entirely to the upward deflection of the wings resulting from the level flight symmetrical air loads.

For the rigid airplane, the contribution to C_{l_β} due to the differential velocities acting on each wing panel was estimated from reference 14 as $C_{l_{\beta_1}}/C_L = -0.129$. Substituting values for a unit angle of attack into equations (B7), (B8), (B9), and (B2) gives

$$\frac{C_{l_{\beta_1}}}{C_L} = -0.129\left(1 - \frac{\frac{0.1451}{0.744}q}{1 + \frac{0.0321}{0.1451}q}\right)$$

$$= -0.129\left(1 - \frac{0.195q}{1 + 0.221q}\right)$$

The dihedral angle, measured in a plane parallel with the YZ plane, was calculated through use of the influence coefficients for symmetrical loads described in reference 1 and, for the flight range of interest, could be expressed as

$$\frac{\Gamma_{\eta=1}}{C_L} = 0.1035q$$

The calculated distribution of dihedral angle, normalized with respect to the value at the tip, is given in the following table:

η	0.383	0.707	0.924
Γ	.520	.900	.992

For the wing at a unit angle of sideslip, these values of dihedral angle represent changes in the wing angle of attack, and the rolling-moment coefficient due to dihedral angle may be determined from equations given previously.

$$\frac{C_{l_{\beta_2}}}{C_L} = -(0.1035q)(0.557)\left(1 - \frac{\frac{0.1197}{0.557}q}{1 + \frac{0.02664}{0.1197}q}\right)$$

$$= -0.0577q\left(1 - \frac{0.214q}{1 + 0.222q}\right)$$

Since only first-order effects have been considered, the changes in dihedral angle due to antisymmetric loads have been neglected.

The total value for the wing contribution to C_{l_β} becomes

$$\frac{C_{l_\beta}}{C_L} = \frac{C_{l_{\beta_1}}}{C_L} + \frac{C_{l_{\beta_2}}}{C_L}$$

$$\frac{C_{l_\beta}}{C_L} = -0.129\left(1 - \frac{0.195q}{1 + 0.221q}\right) - 0.0577q\left(1 - \frac{0.214q}{1 + 0.222q}\right) \qquad \text{(B10)}$$

While the two load distributions yield somewhat different values of the ratio C_{l_A}/C_{l_R}, the values of k are essentially the same. This was also found to be true for other types of load distributions. Note that the values of C_{l_β} obtained from equation (B10) are not the same as those given in table III since only the contribution of the wing has been considered here.

REFERENCES

1. Cole, Henry A., Jr., Brown, Stuart C., and Holleman, Euclid C.: Experimental and Predicted Longitudinal Response Characteristics of a Large Flexible 35° Swept-Wing Airplane at an Altitude of 35,000 Feet. NACA RM A54H09, 1954.

2. Cole, Henry A., Jr., Brown, Stuart C., and Holleman, Euclid C.: The Effects of Flexibility on the Longitudinal and Lateral-Directional Response of a Large Airplane. NACA RM A55D14, 1955.

3. Spencer, C. P., and Ritchey, W. M., Jr.: Dynamic Response of the B-47 Airplane in Flight. WADC TN 54-113, Wright Air Development Center, Oct. 1955.

4. Triplett, William C., Brown, Stuart C., and Smith, G. Allan: The Dynamic-Response Characteristics of a 35° Swept-Wing Airplane as Determined From Flight Measurements. NACA Rep. 1250, 1955.

5. Brown, R. B., and Perkins, Grace: Full Scale Test of the XB-47 Empennage. Part II - Pressure Data. Boeing Airplane Co. Document No. D-8517-1, Oct. 27, 1948.

6. White, Roland J.: Investigation of Lateral Dynamic Stability in the XB-47 Airplane. Jour. Aero. Sci., vol. 17, no. 3, Mar. 1950, pp. 133-148.

7. Swenson, Floyd: Fin and Rudder Destruction Tests, Model B-47B. Boeing Airplane Co., Test No. 25308, Apr. 18, 1951.

8. Mayo, Alton P., and Ward, John F.: Experimental Influence Coefficients for the Deflection of the Wing of a Full-Scale, Swept-Wing Bomber. NACA RM L53L23, 1954.

9. Schumacher, Lloyd E.: Methods for Analyzing Transient Flight Data to Obtain Aircraft Frequency Response. AF, Air Materiel Command, Wright-Patterson AFB (Flight Test Div. Memo Rep.) Ser. MCRFT - 2268, 17 Jan. 1950.

10. Andrew, G. M.: End Correction for Flight-Tested Frequency Response Obtained by Laplace Transformation. Jour. Aero. Sci., vol. 19, no. 8, Aug. 1952, pp. 569-570.

11. Flutter Inspection of Boeing XB-47 Airplane. AF, Air Materiel Command, Wright-Patterson AFB (Eng. Div. Memo Rep.) Ser. MCREXA5-4262-36-29, 9 Jan. 1948.

12. DeYoung, John: Theoretical Antisymmetric Span Loading for Wings of Arbitrary Plan Form at Subsonic Speeds. NACA Rep. 1056, 1951.

13. Miles, John W.: The Rolling Moment Due to Sideslip for a Swept Wing. Jour. Aero. Sci., vol. 15, no. 7, July 1948, pp. 418-424.

14. Holtby, K., and Seiler, R.: Development of Lateral Controls for Flexible Swept Wings. Boeing Airplane Co. Document No. D-9458, Apr. 6, 1950.

TABLE I.- PHYSICAL CHARACTERISTICS OF THE TEST AIRPLANE

Wing	
Area, sq ft	1428
Span, ft	116
Aspect ratio	9.43
Taper ratio	0.42
Mean aerodynamic chord, ft	13.0
Sweepback of quarter-chord line, deg	35
Airfoil thickness ratio (parallel to body center line), percent	12
Dihedral, deg	0
Ailerons	
Area aft of hinge center line (each), sq ft	53.8
Aileron span to wing span ratio	0.405
Average aileron chord to wing chord ratio	0.26
Vertical tail	
Area (including dorsal), sq ft	227
Span, ft	18.7
Aspect ratio	1.54
Taper ratio	0.34
Mean aerodynamic chord, ft	13.02
Sweepback of quarter-chord line, deg	34.9
Airfoil thickness ratio (parallel to body center line), percent	10
Distance 1/4-chord wing M.A.C. to 1/4-chord vertical tail M.A.C., ft	46.5
Rudder	
Area aft of hinge center line, sq ft	51.2
Average rudder chord to vertical tail chord ratio	0.30
Average gross weight, lb	115,000
Moment of inertia about the X axis, slug-ft^2	1,074,000
Moment of inertia about the Z axis, slug-ft^2	2,306,000
Inclination of principal longitudinal axis with respect to fuselage reference line, deg	-2.6

TABLE II.- STRUCTURAL INFLUENCE COEFFICIENTS

(a) Wing

		1000-pound load at station							
		3F	3R	2F	2R	1F	1R	5F	5R
Inches deflection at station	3F	0.0659	0.0580	0.1765	0.1663	0.2447	0.2307	0.2033	0.1936
	3R	.0705	.0931	.2116	.2398	.3057	.3339	.2486	.2784
	2F	.1769	.2052	.7419	.7795	1.2134	1.2490	.9285	.9590
	2R	.1804	.2318	.7881	.9005	1.3309	1.4300	.9995	1.1070
	1F	.2302	.2730	1.1943	1.2934	2.3486	2.3840	1.6374	1.7184
	1R	.2330	.2940	1.2430	1.4057	2.4598	2.5920	1.7086	1.8677

(b) Fuselage

Load	Average change in vertical tail yaw angle due to fuselage and tail flexibility, deg	Change in yaw angle at tail turn meter, deg	Change in roll angle at tail turn meter, deg
1000 pound aerodynamic load due to sideslip of vertical tail	0.0685	0.0342	-0.0798
1000 pound aerodynamic load due to rudder deflection	-.0808	-.0402	.0942
1g lateral acceleration	.581	.290	---
1 radian/sec^2 yawing acceleration	-.832	-.415	---

Note: Wing station locations are shown in figure 5. The letter F denotes front spar location; R denotes rear spar location.

TABLE III.- LATERAL-DIRECTIONAL STABILITY DERIVATIVES PREDICTED FROM WIND-TUNNEL DATA AND AVAILABLE THEORY; h = 35,000 FEET, W = 115,000 POUNDS

Quantity	Flexible				Rigid			
M	0.5	0.6	0.7	0.8	0.5	0.6	0.7	0.8
q	87.2	125.5	171.0	223.1	87.2	125.5	171.0	223.1
C_L	.922	.642	.471	.361	.922	.642	.471	.361
C_{l_p}	-.430	-.429	-.427	-.426	-.490	-.507	-.540	-.570
C_{n_p}	-.0960	-.0660	-.0470	-.0350	-.0994	-.0692	-.0507	-.0389
C_{l_r}	.215	.136	.090	.060	.264	.184	.135	.104
C_{n_r}	-.142	-.137	-.134	-.130	-.150	-.150	-.150	-.150
C_{l_β}	-.170	-.141	-.122	-.112	-.157	-.129	-.113	-.101
C_{n_β}	.110	.106	.102	.098	.120	.120	.120	.120
C_{Y_β}	-.575	-.566	-.555	-.544	-.600	-.600	-.600	-.600
$C_{l_{\delta_r}}$	.0052	.0090	.0109	.0122	.0057	.0095	.0119	.0135
$C_{n_{\delta_r}}$	-.0724	-.0700	-.0672	-.0645	-.0778	-.0778	-.0778	-.0778
$C_{Y_{\delta_r}}$	.183	.180	.175	.171	.194	.194	.194	.194
$C_{l_{\delta_a}}$	.0594	.0528	.0462	.0392	.0770	.0770	.0770	.0770
$C_{n_{\delta_a}}$	-.0103	-.0064	-.0041	-.0027	-.0133	-.0093	-.0068	-.0052
r_X	-.116	-.059	-.005	.031	-.103	-.047	-.010	.014
r_Z	-.048	-.021	-.005	.007	-.047	-.020	-.005	.007

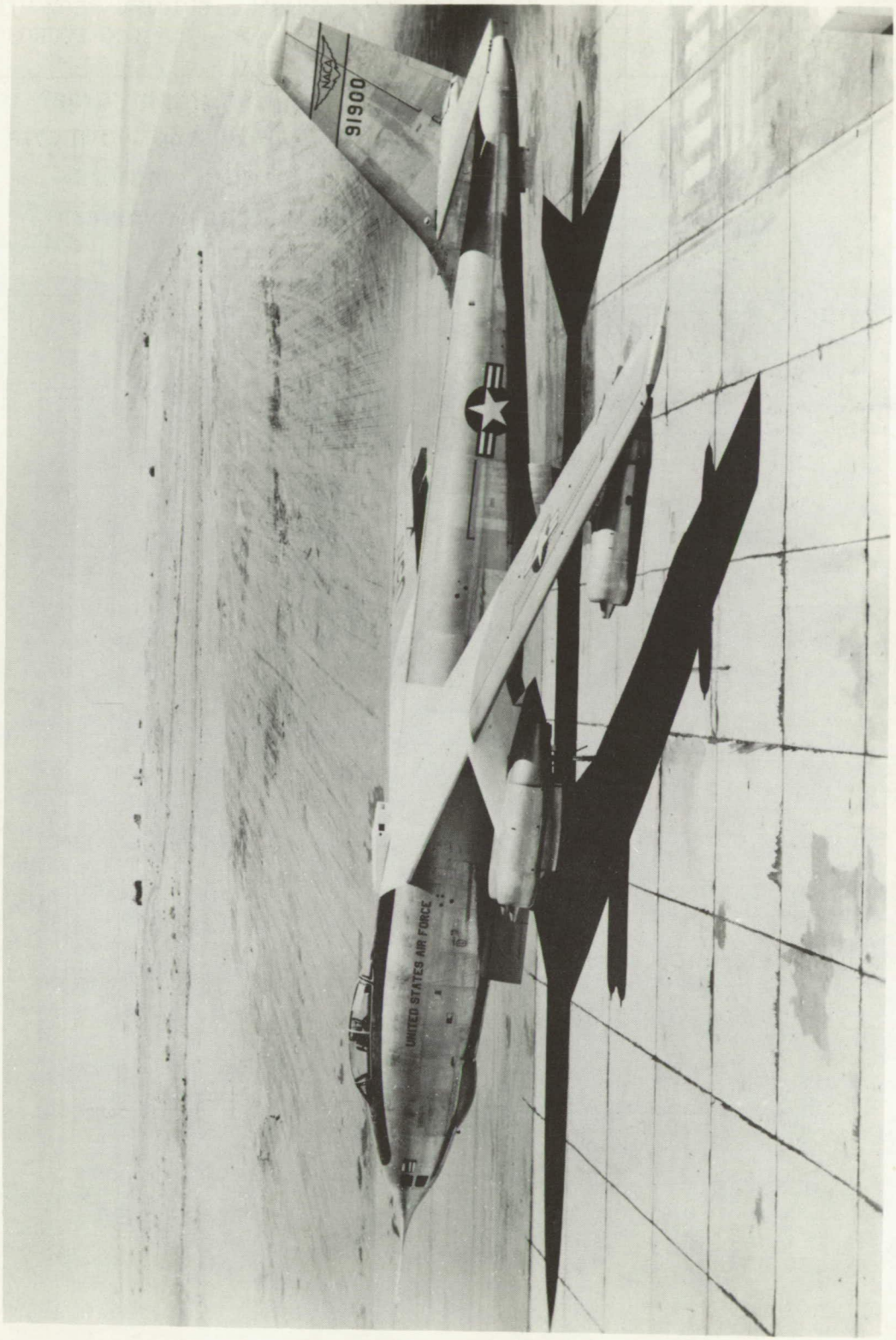

A-19582

Figure 1.- Photograph of the test airplane.

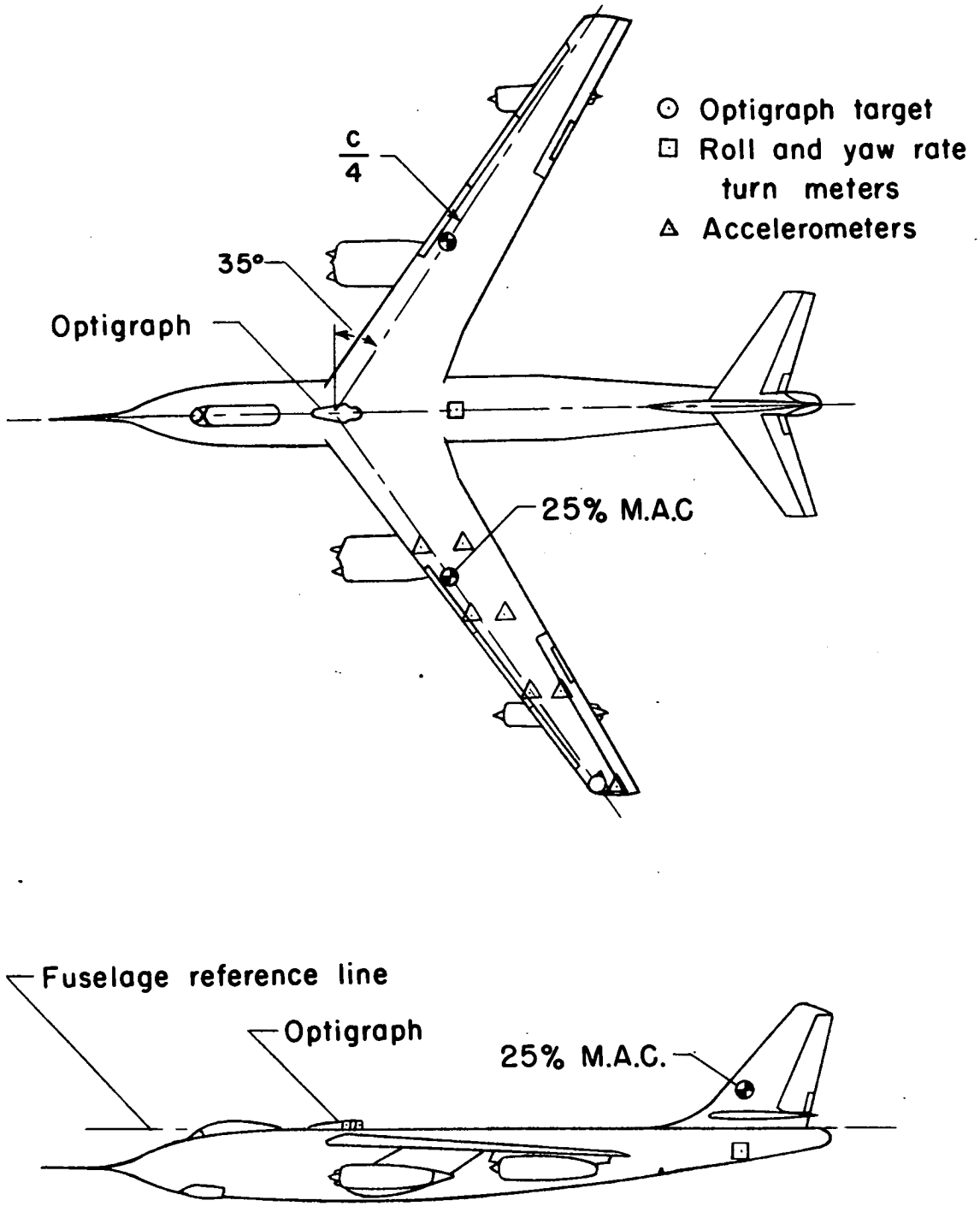

Figure 2.- Two-view drawing of test airplane.

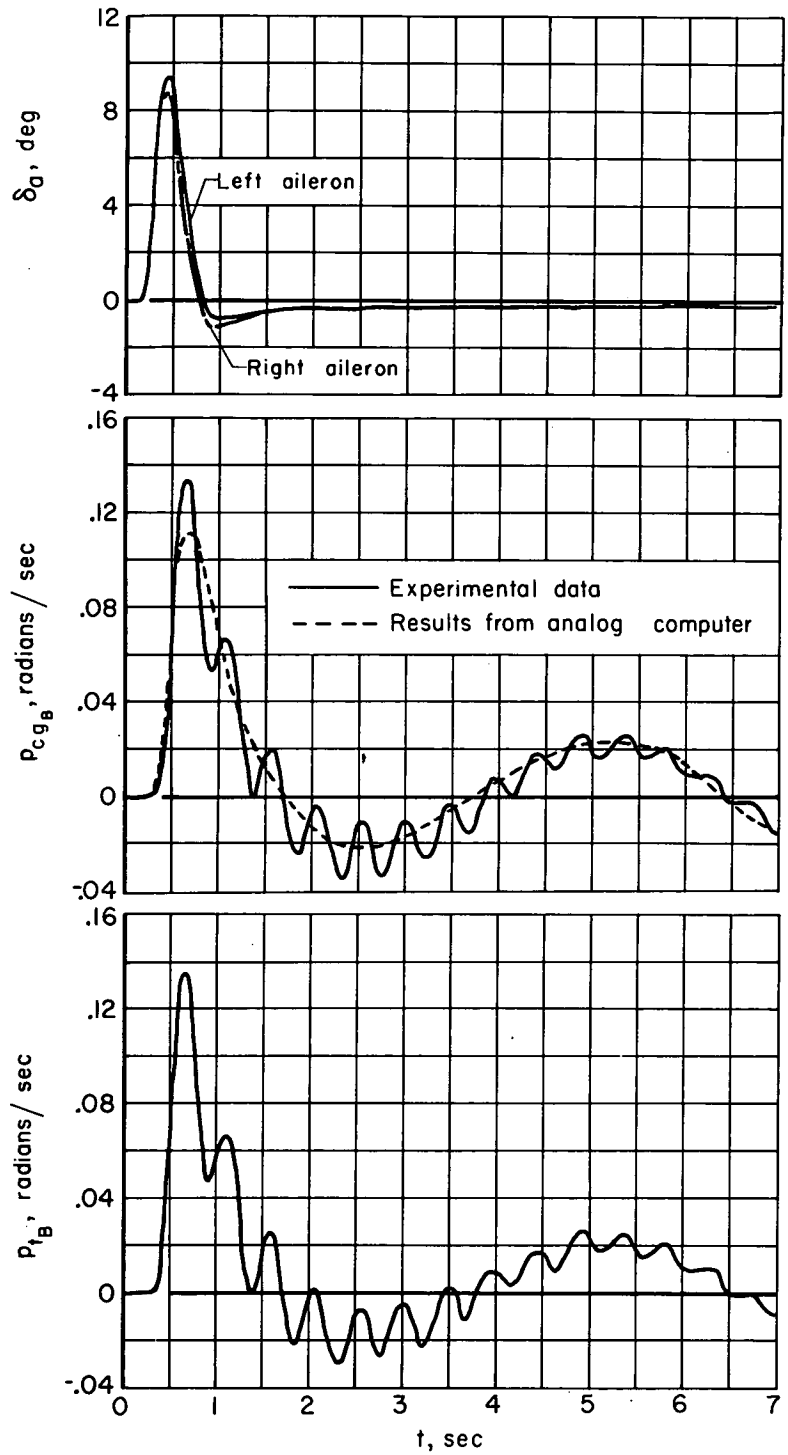

(a) Time histories of δ_a, p_{cg_B}, and p_{t_B}.

Figure 3.- Typical time histories for aileron pulse; M = 0.71.

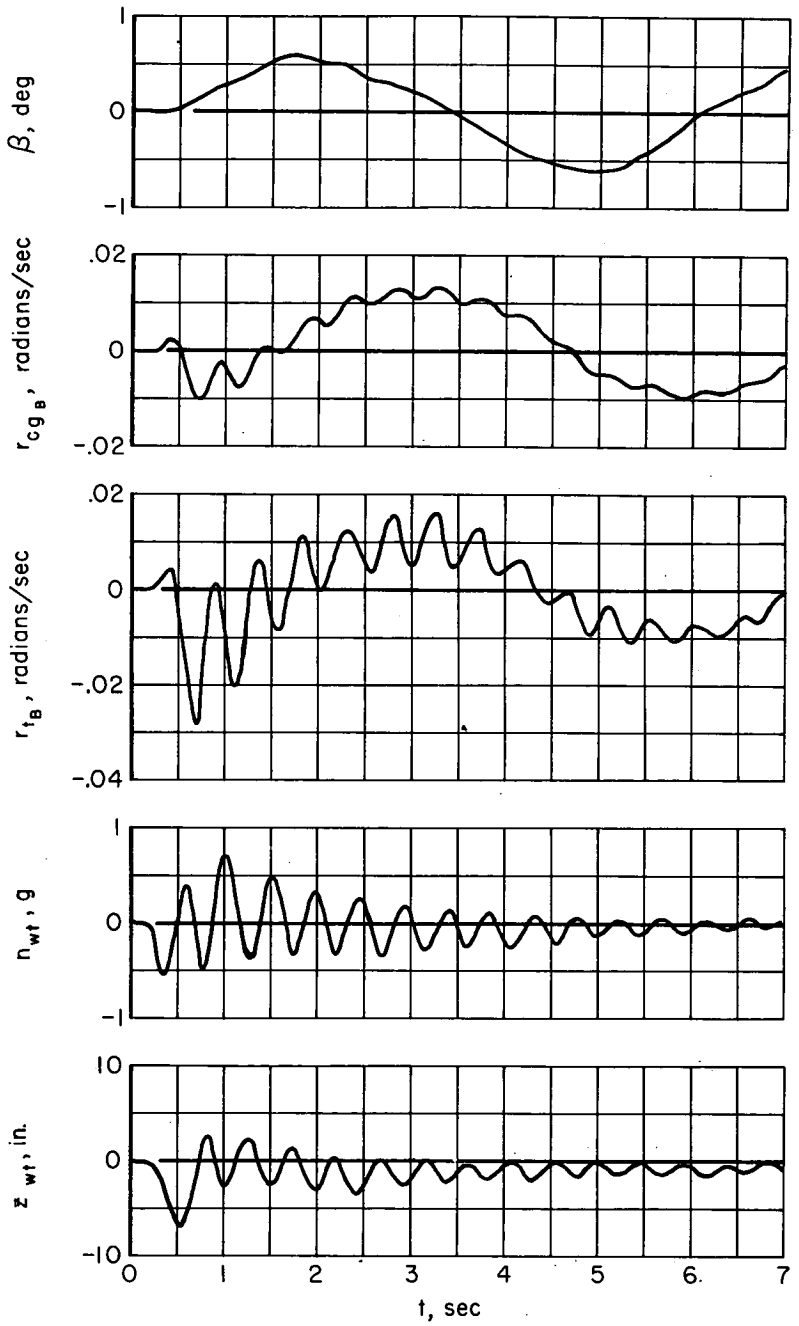

(b) Time histories of β, r_{cg_B}, r_{t_B}, n_{wt}, and z_{wt}.

Figure 3.- Concluded.

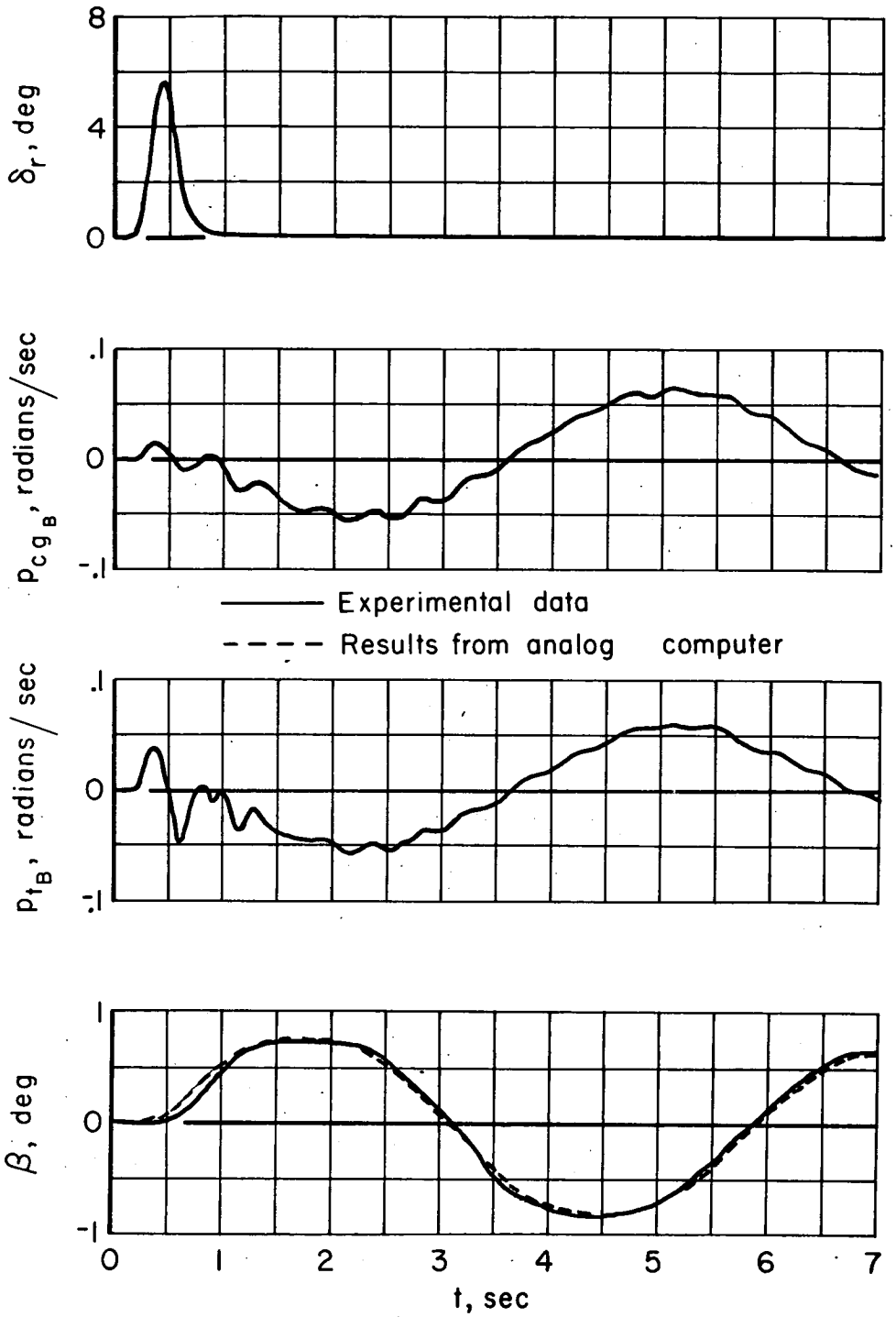

(a) Time histories of δ_r, p_{cg_B}, p_{t_B}, and β.

Figure 4.- Typical time histories for rudder pulse; M = 0.71.

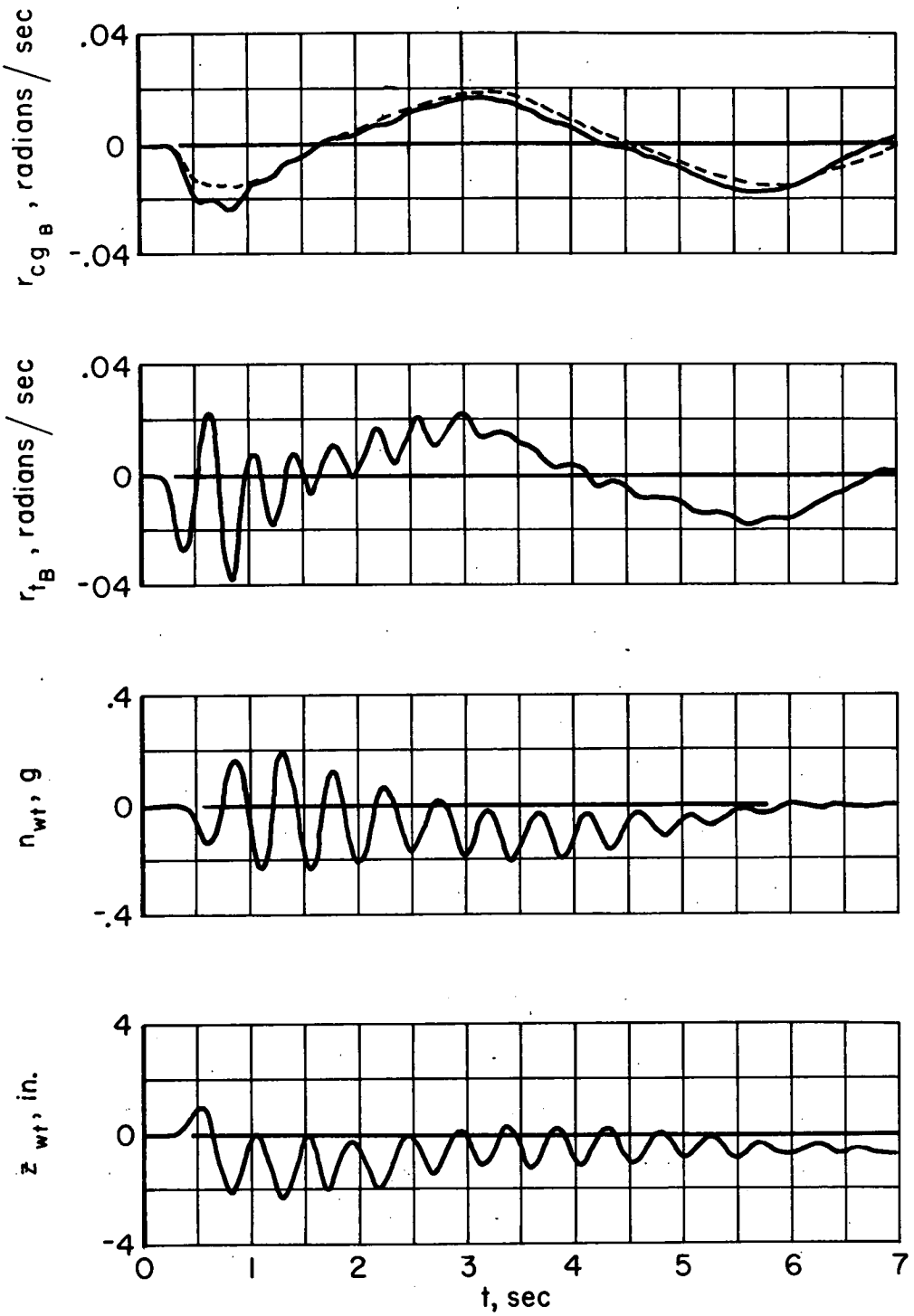

(b) Time histories of r_{cg_B}, r_{t_B}, n_{wt}, and z_{wt}.

Figure 4.- Continued.

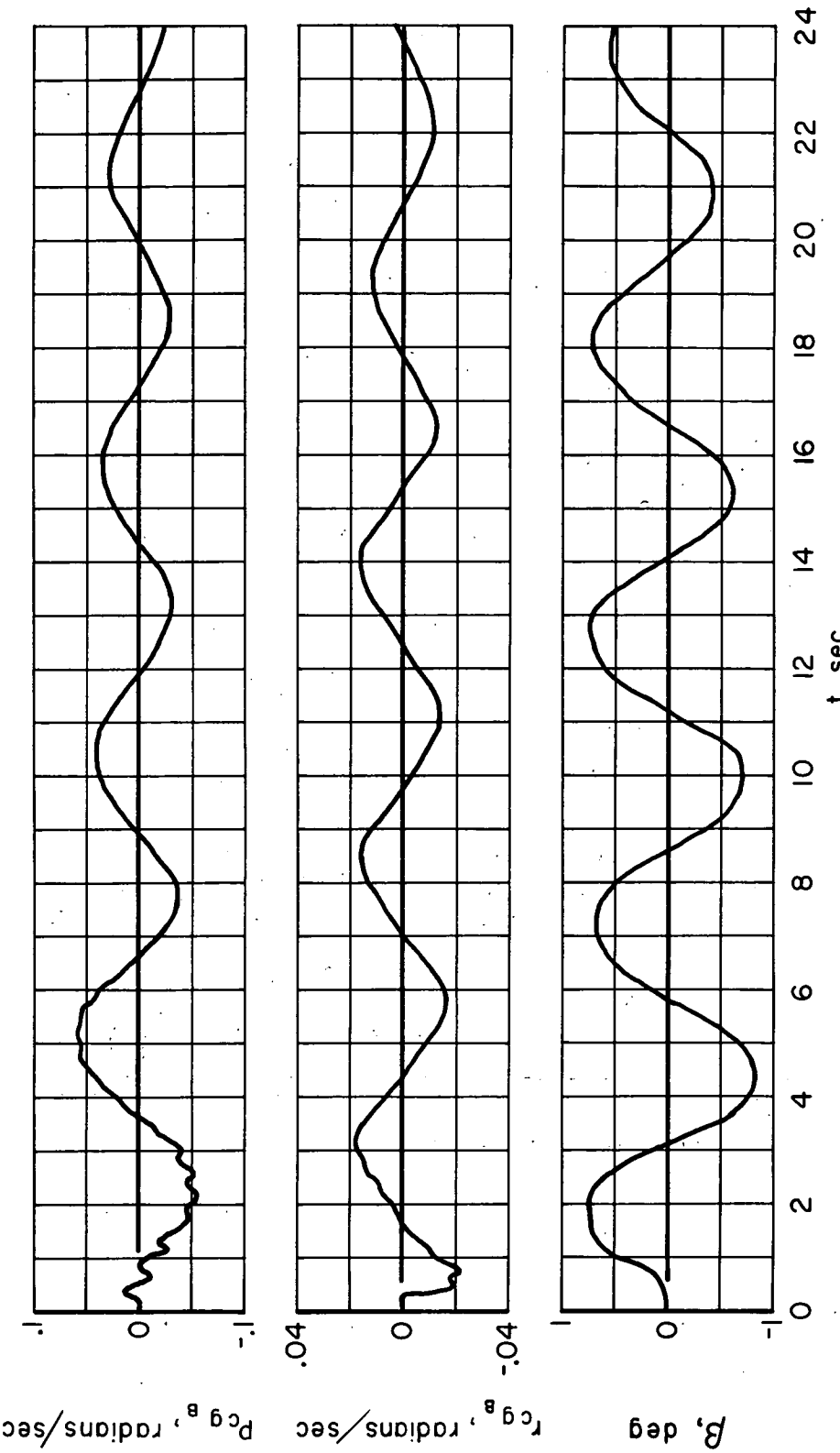

(c) Complete time histories of p_{cg_B}, r_{cg_B}, and β.

Figure 4.- Concluded.

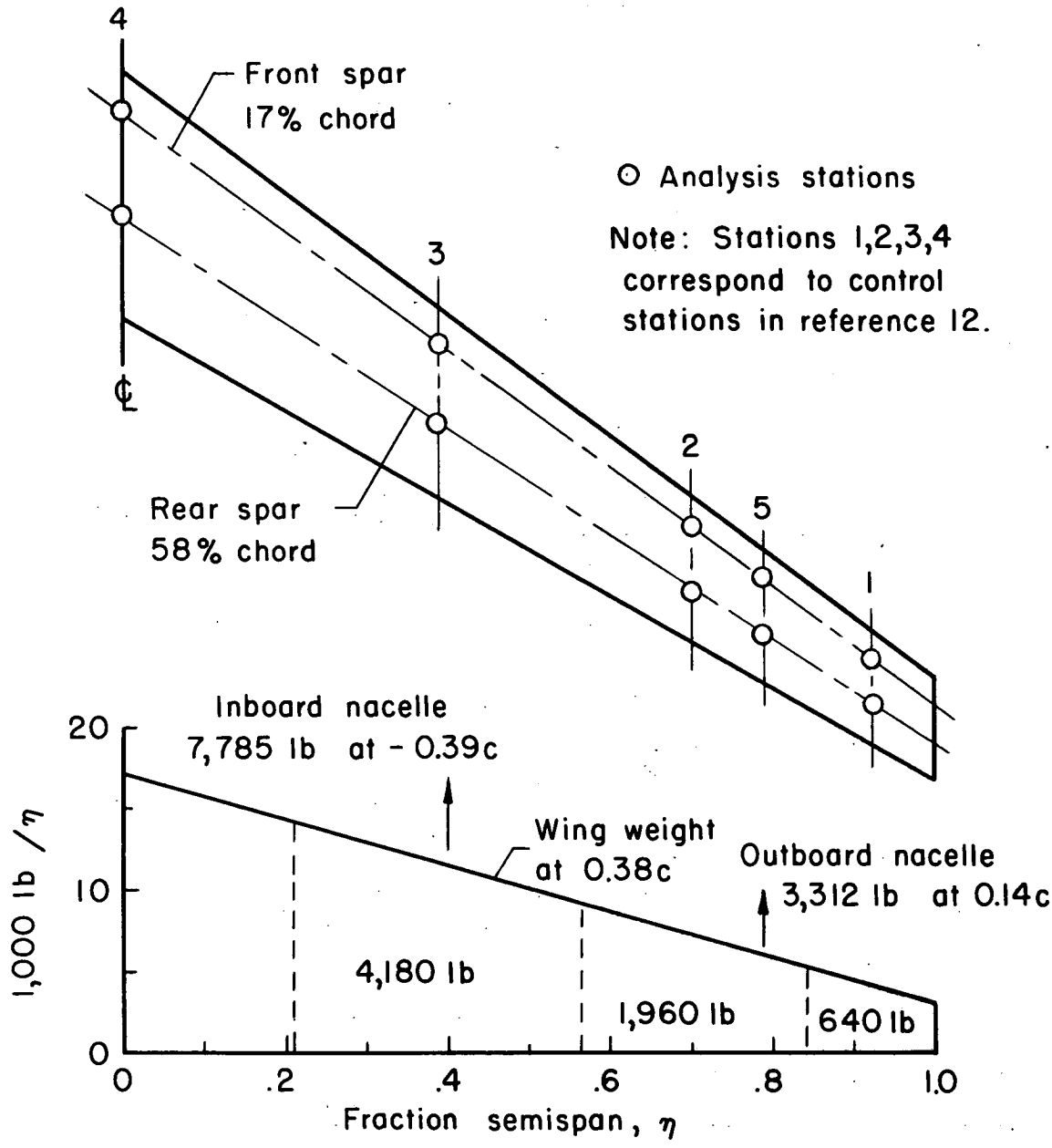

Figure 5.- Wing stations and weight distribution used in analysis.

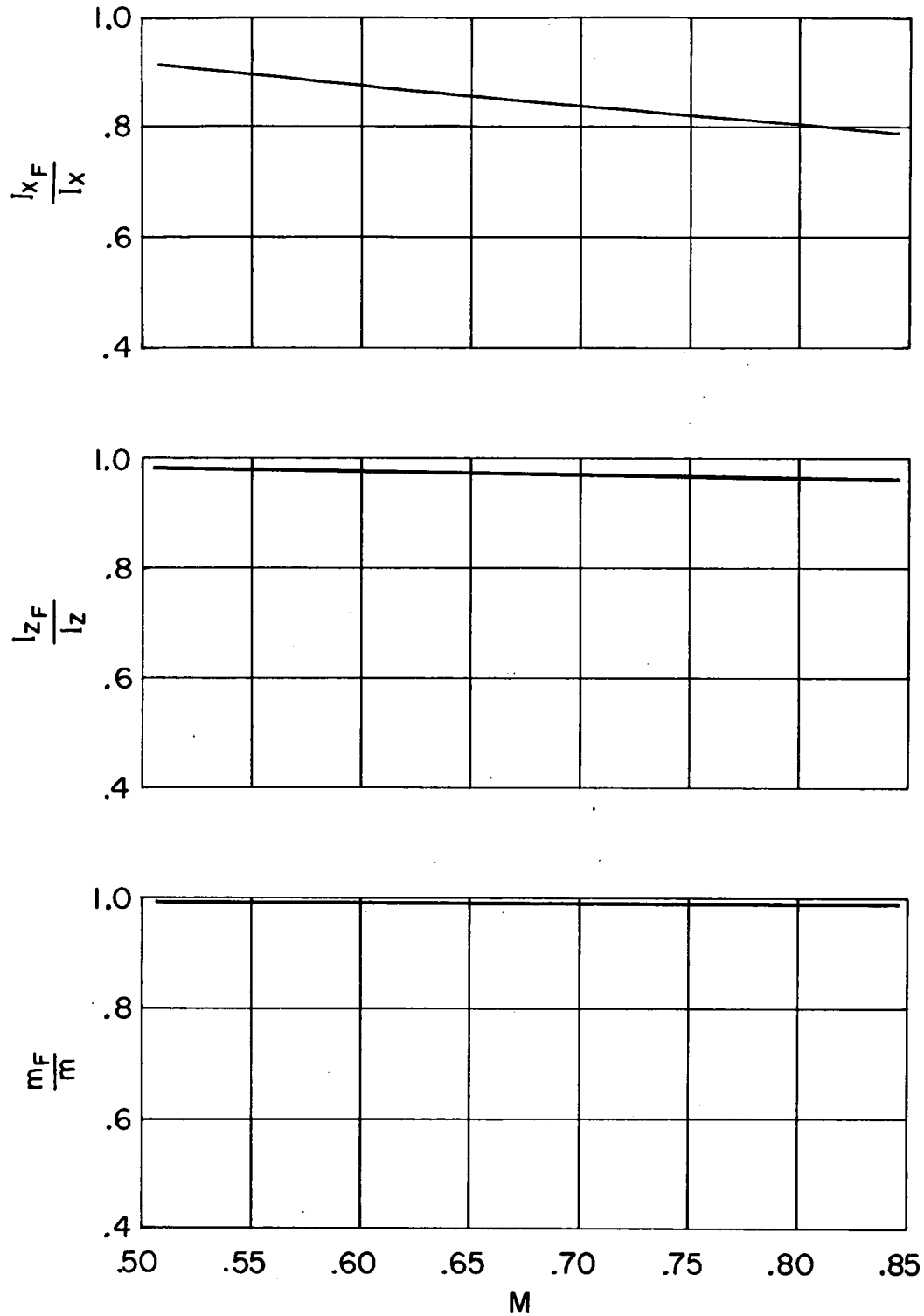

Figure 6.- Influence of flexibility on effective inertia characteristics.

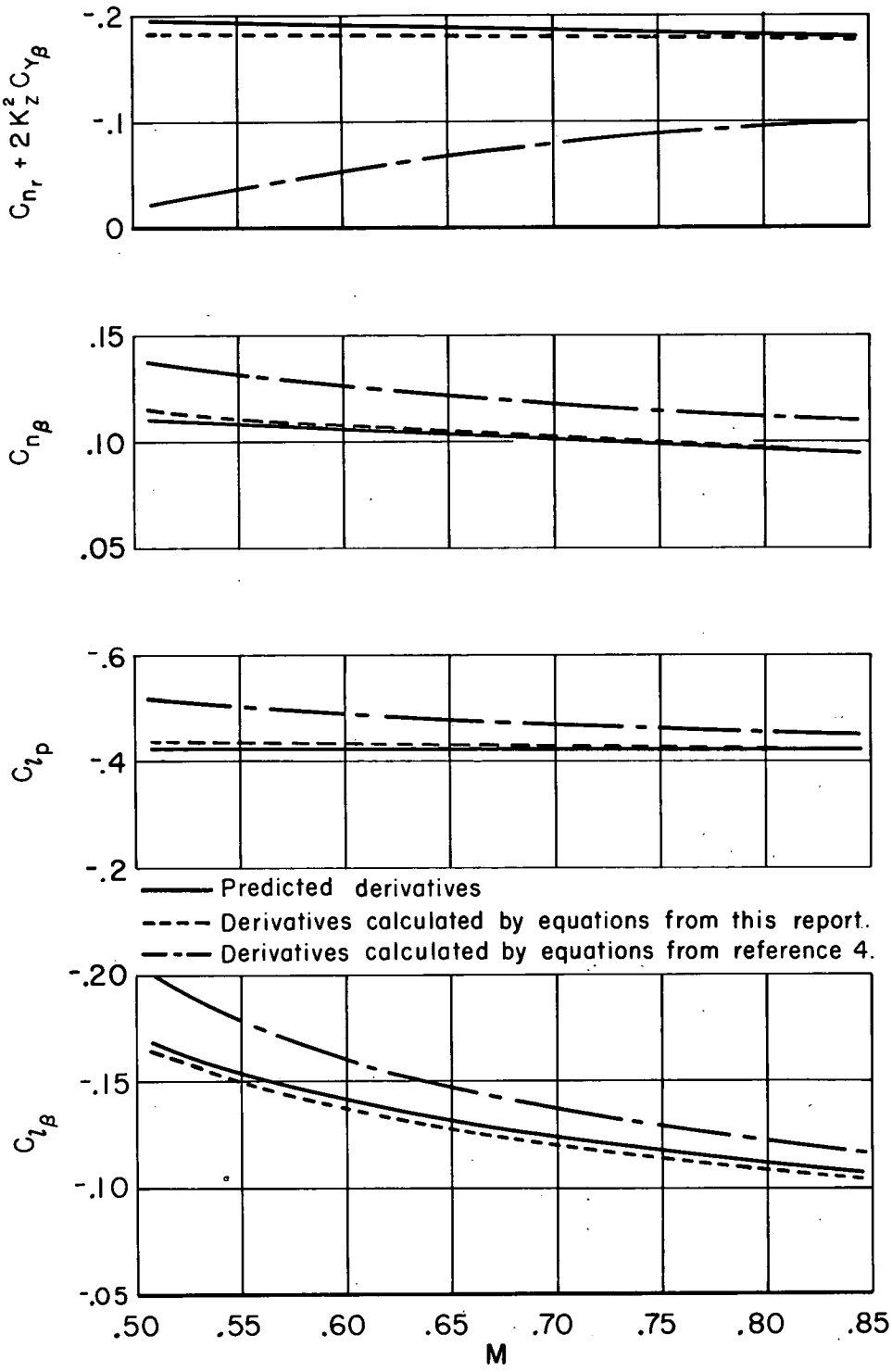

Figure 7.- Comparison of predicted aerodynamic derivatives for the flexible airplane with those calculated from predicted transfer-function coefficients using approximate equations.

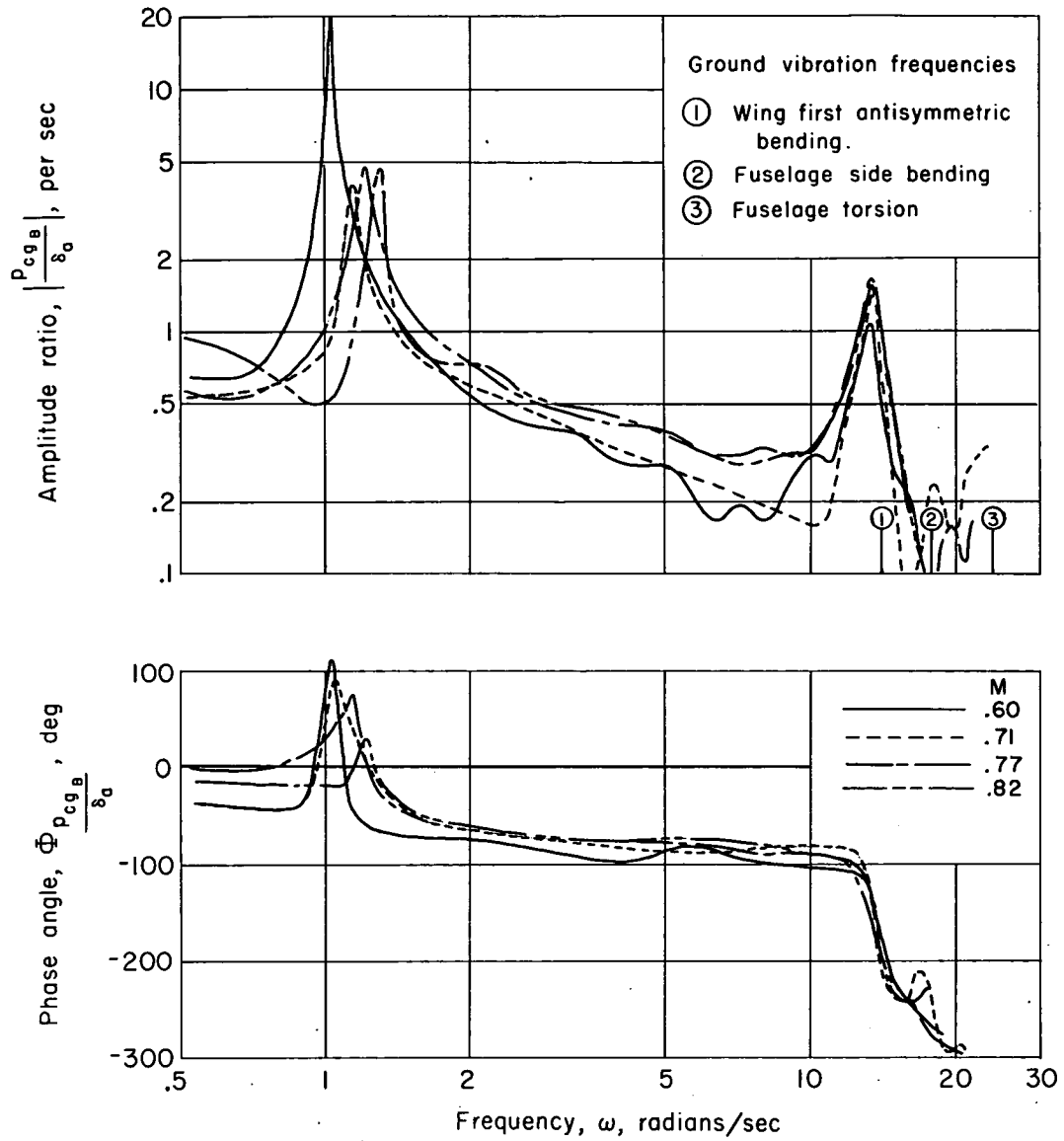

(a) Rolling velocity at the center of gravity.

Figure 8.- Frequency responses to aileron inputs at various Mach numbers.

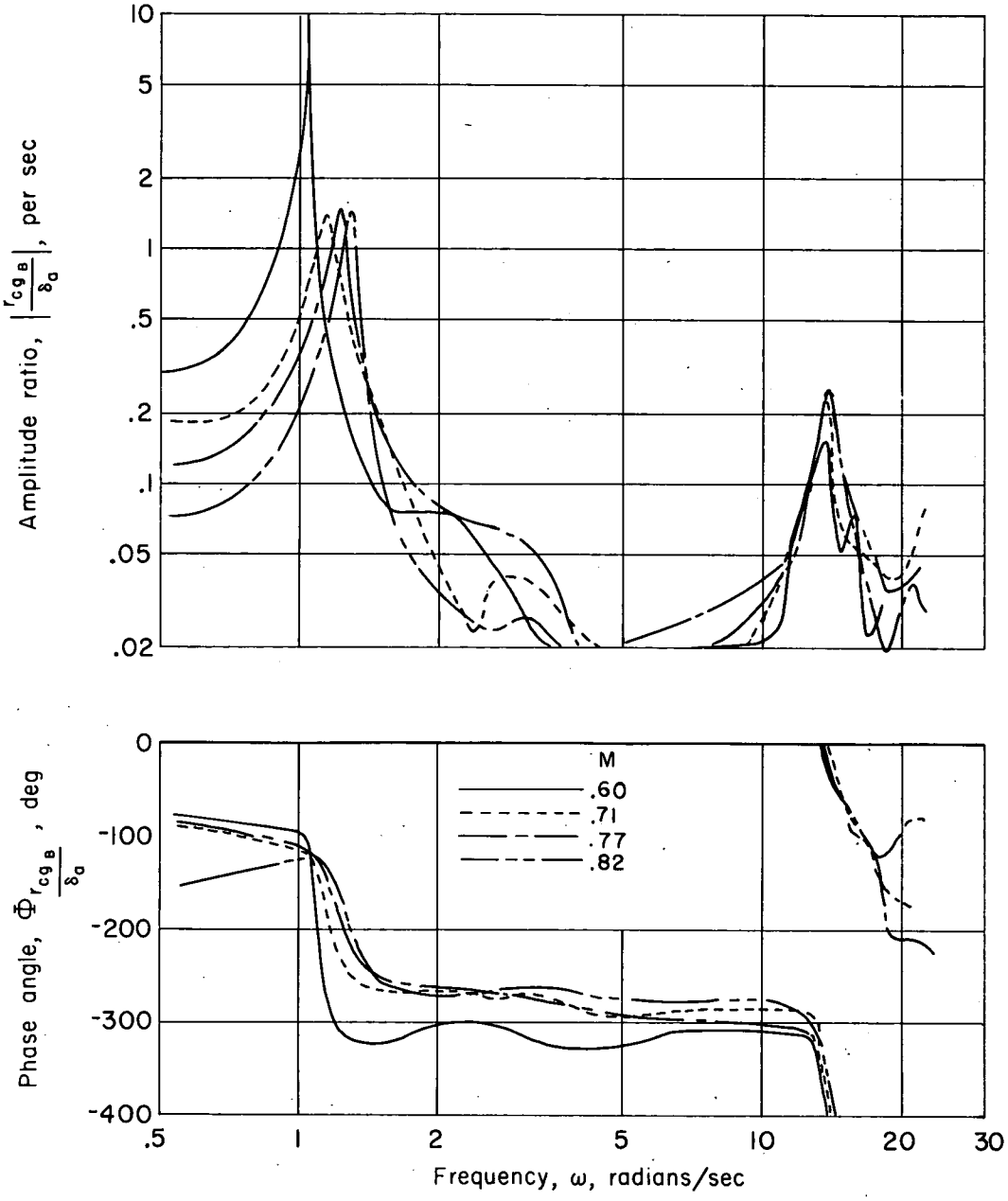

(b) Yawing velocity at the center of gravity.

Figure 8.- Continued.

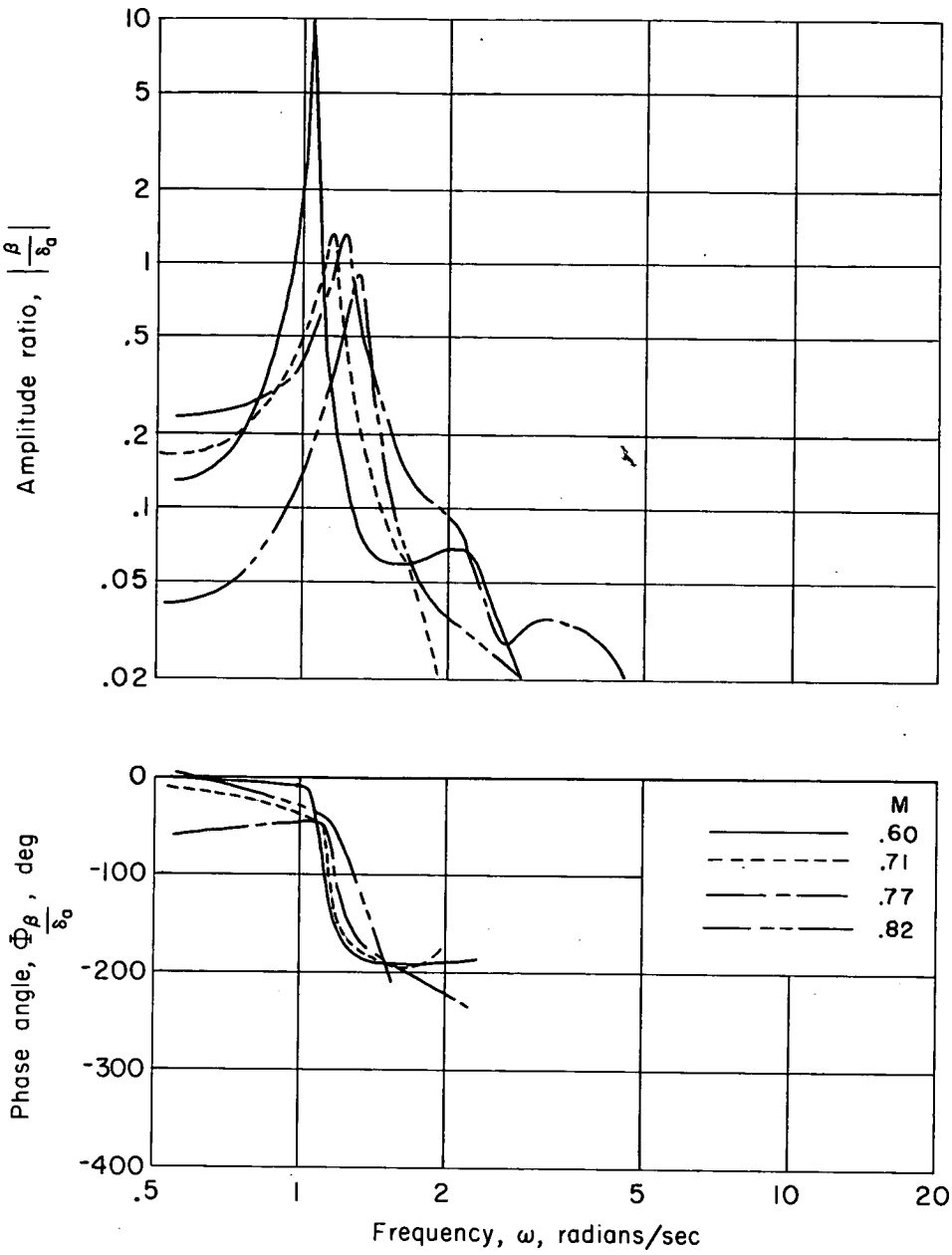

(c) Sideslip angle.

Figure 8.- Continued.

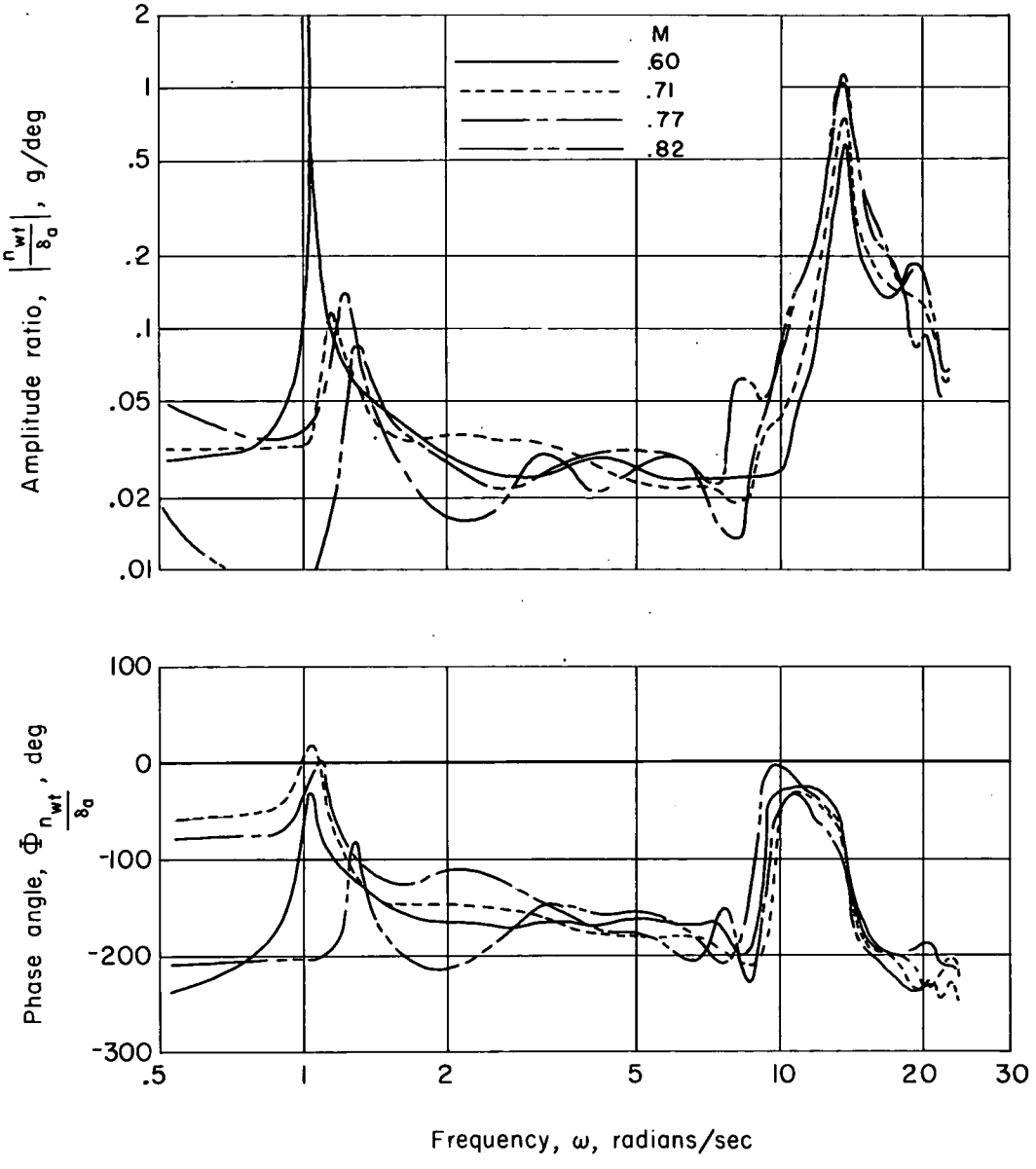

(d) Wing-tip acceleration.

Figure 8.- Concluded.

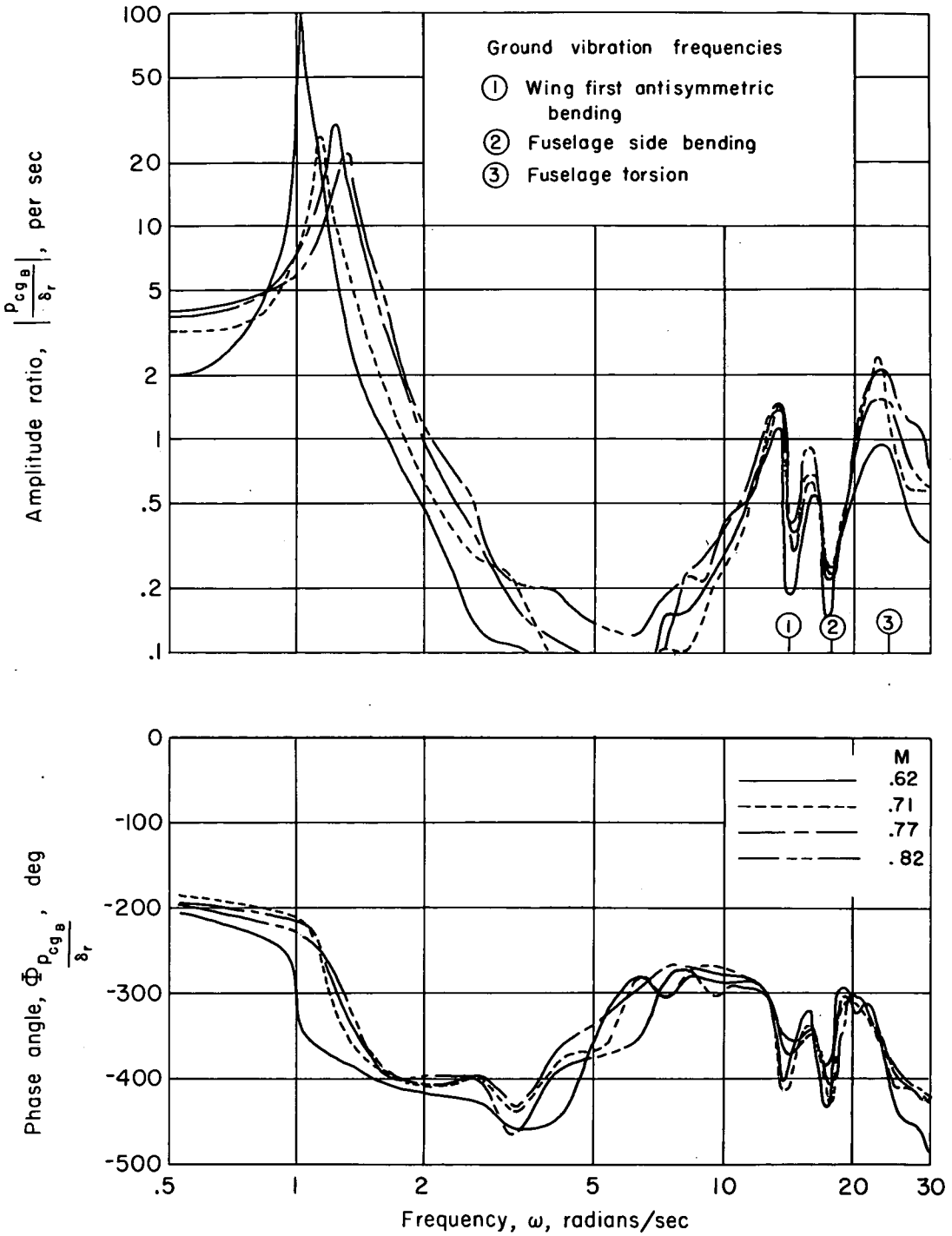

(a) Rolling velocity at the center of gravity.

Figure 9.- Frequency responses to rudder inputs at various Mach numbers.

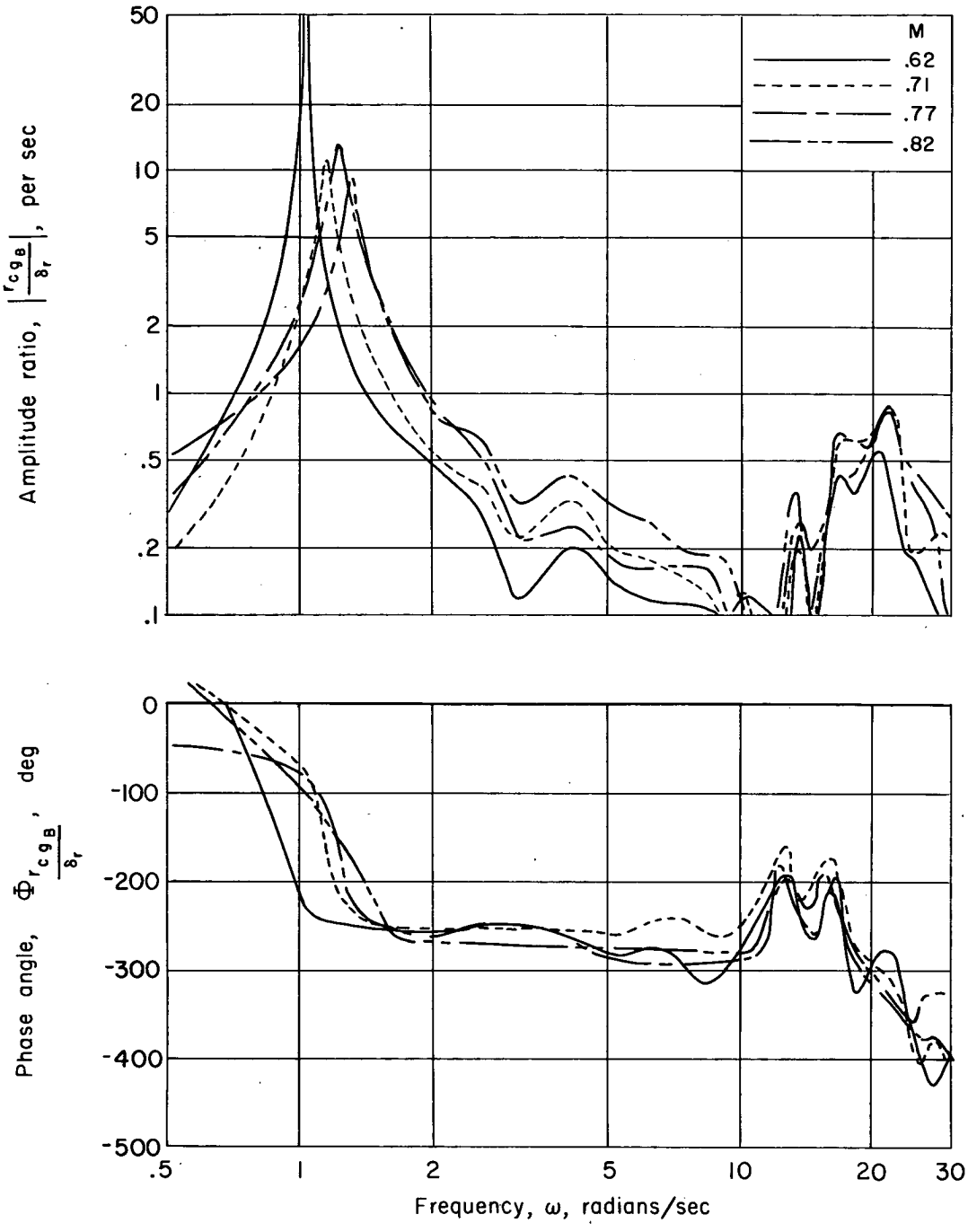

(b) Yawing velocity at the center of gravity.

Figure 9.- Continued.

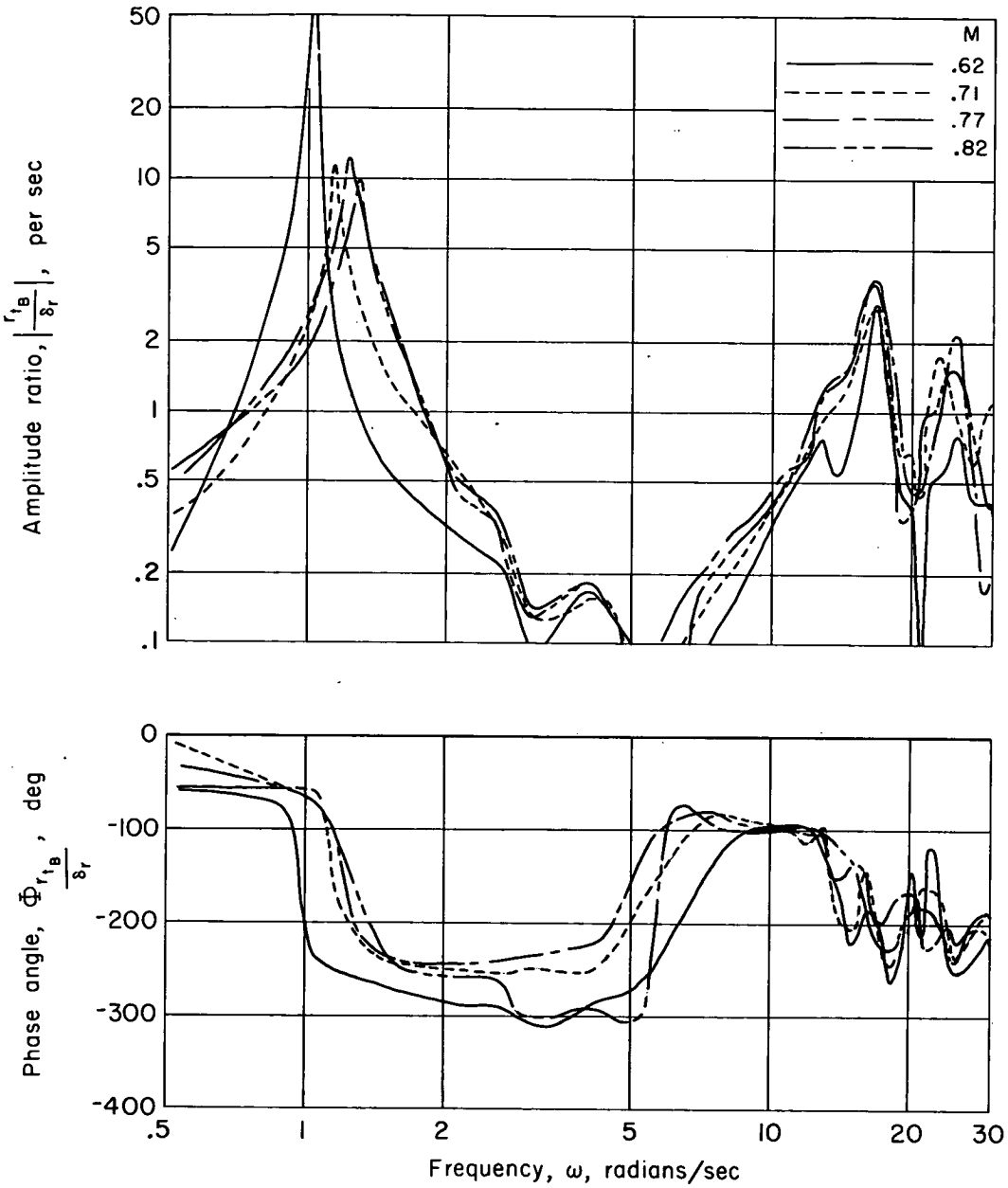

(c) Yawing velocity at the tail.

Figure 9.- Continued.

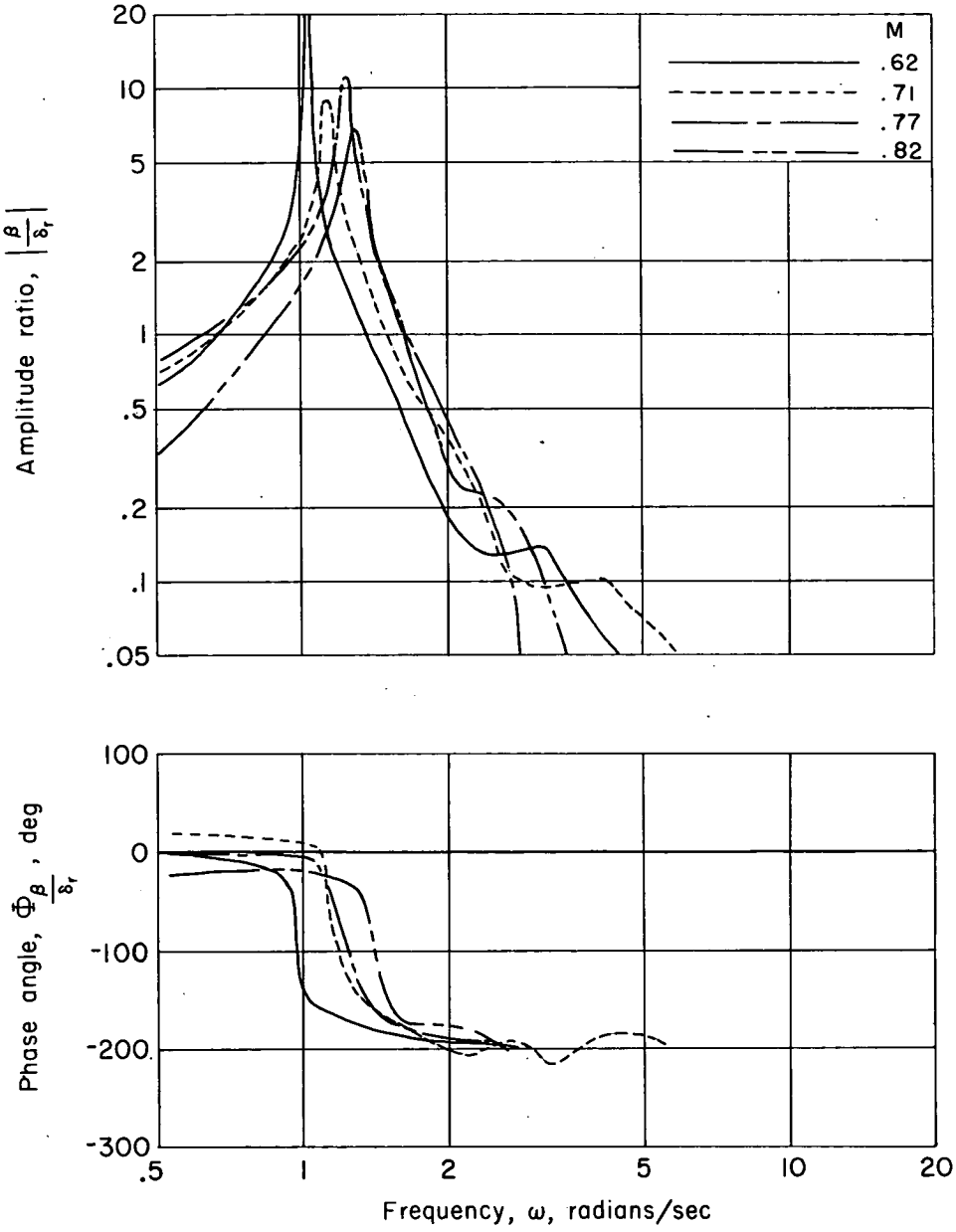

(d) Sideslip angle.

Figure 9.- Continued.

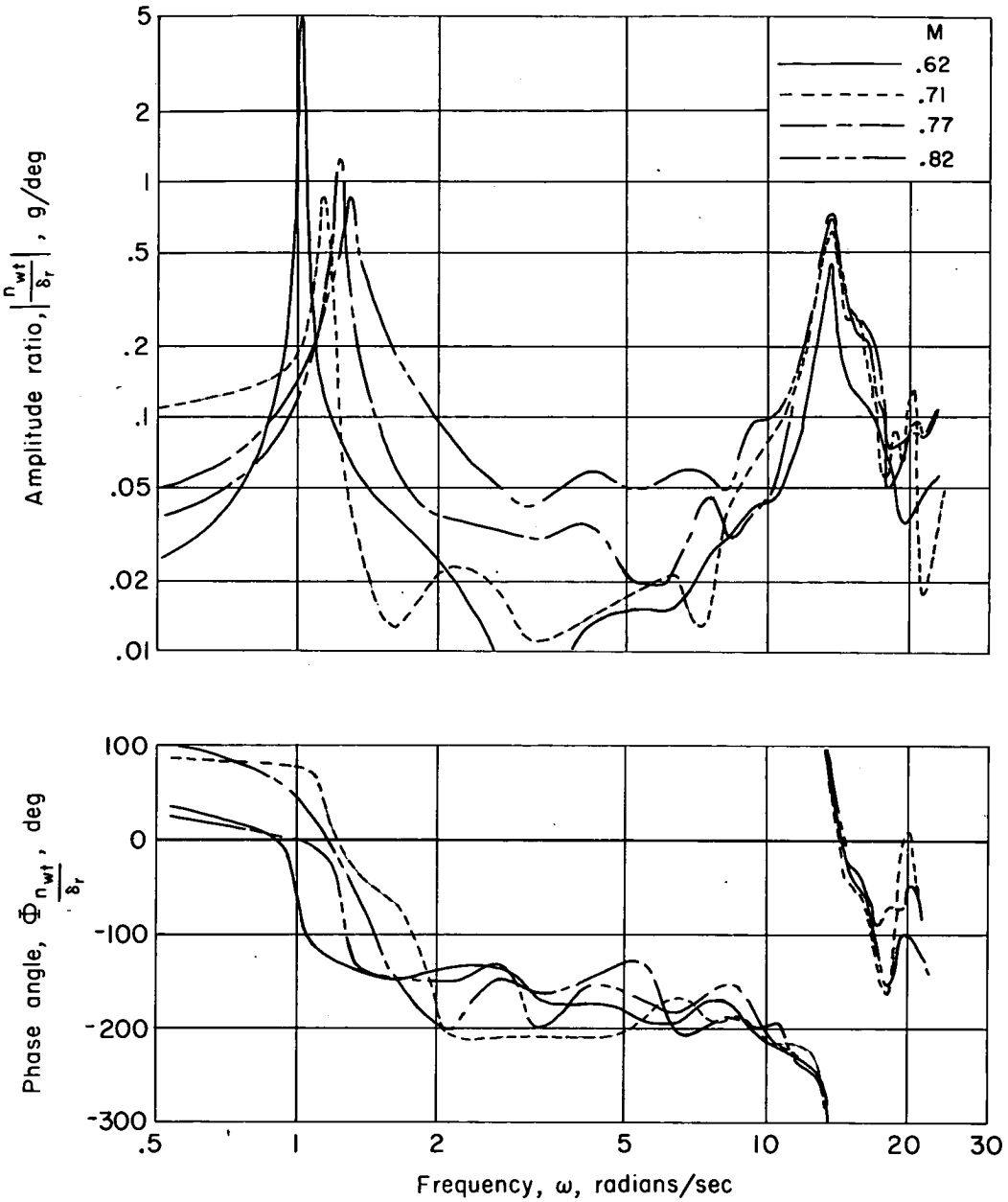

(e) Wing-tip acceleration.

Figure 9.- Concluded.

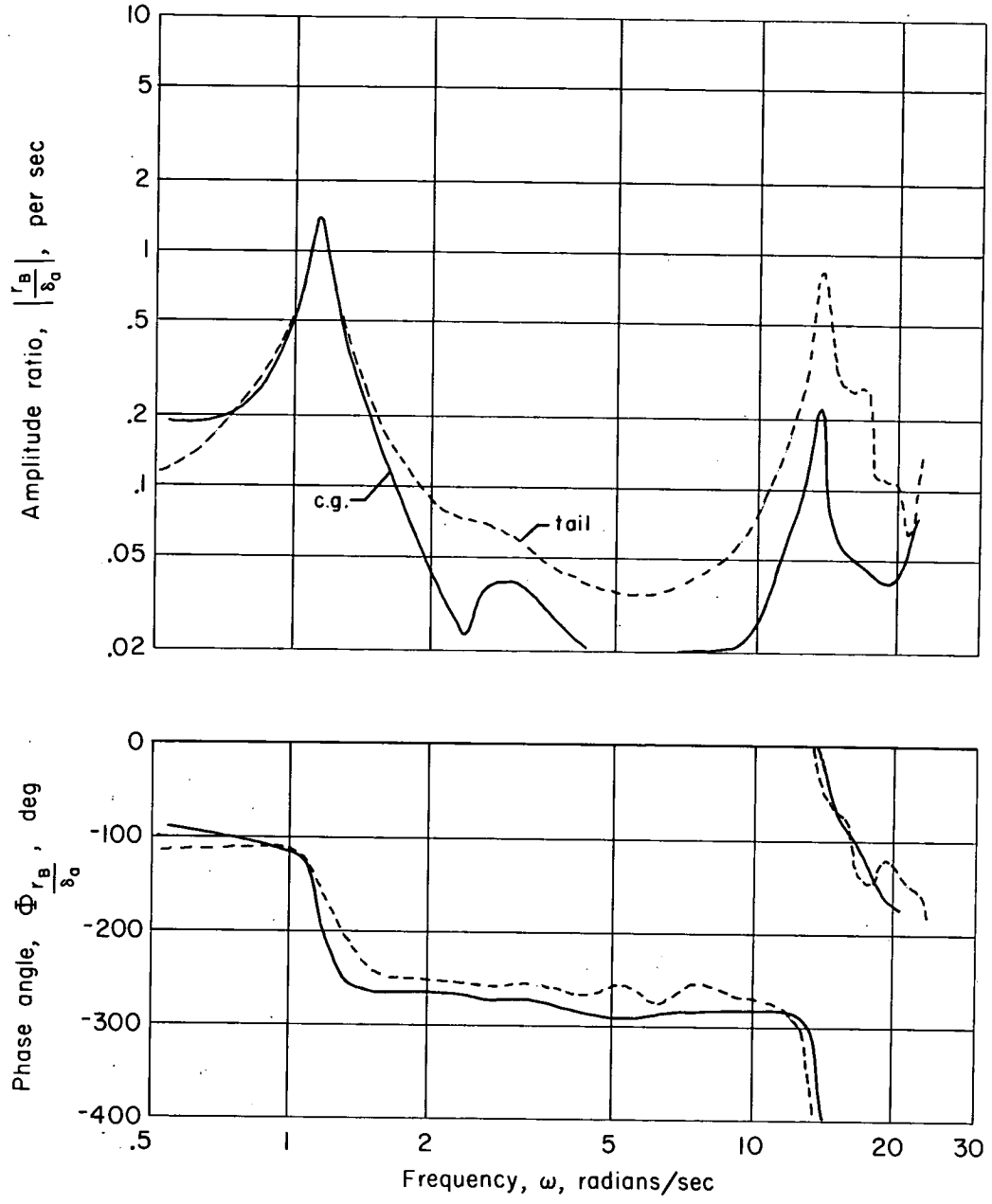

Figure 10.- Comparison of the measured yawing velocity frequency responses at the center of gravity and the tail to an aileron input; M = 0.71.

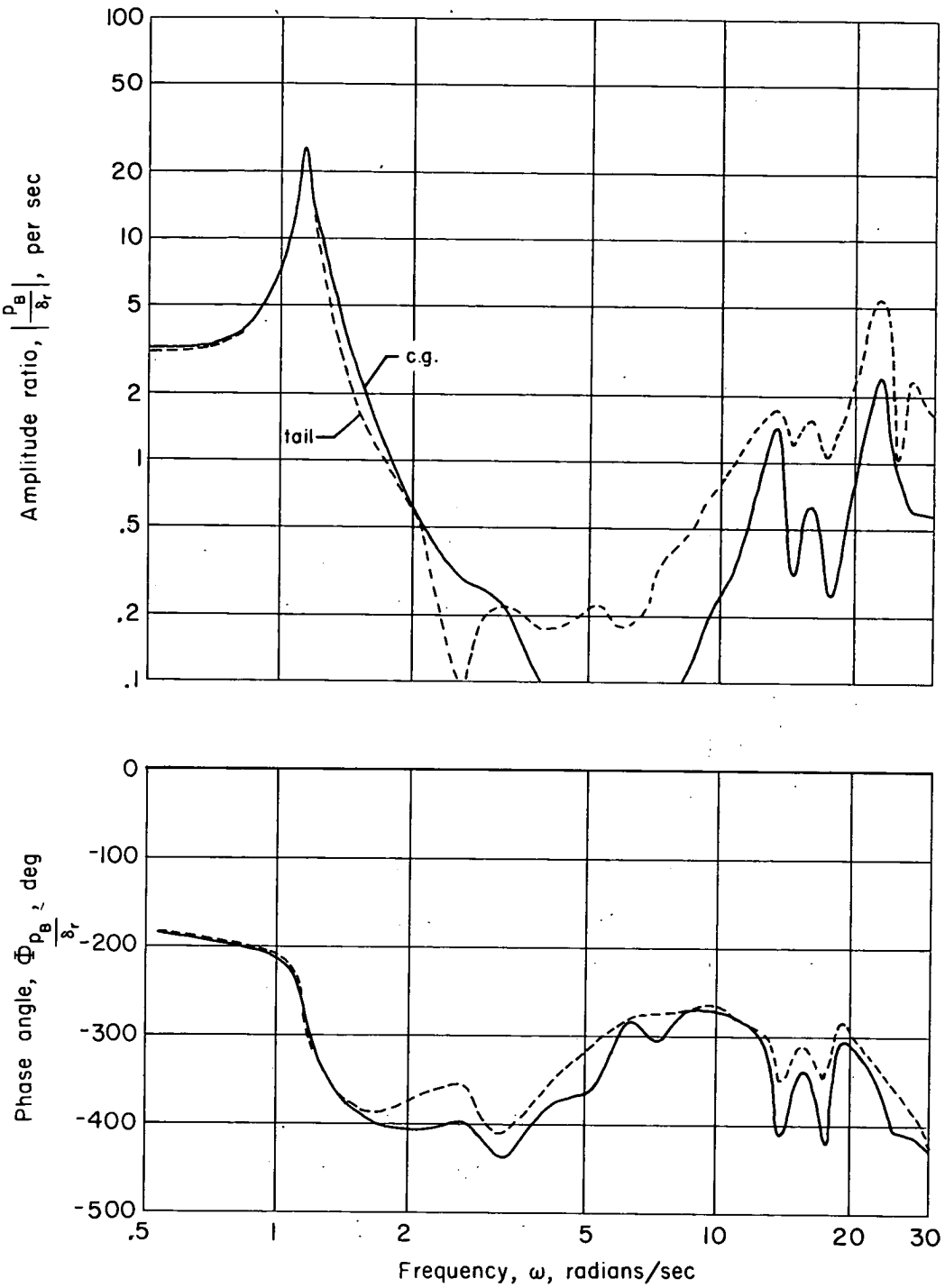

(a) Rolling velocity.

Figure 11.- Comparison of measured frequency responses at the center of gravity and the tail to a rudder input; M = 0.71.

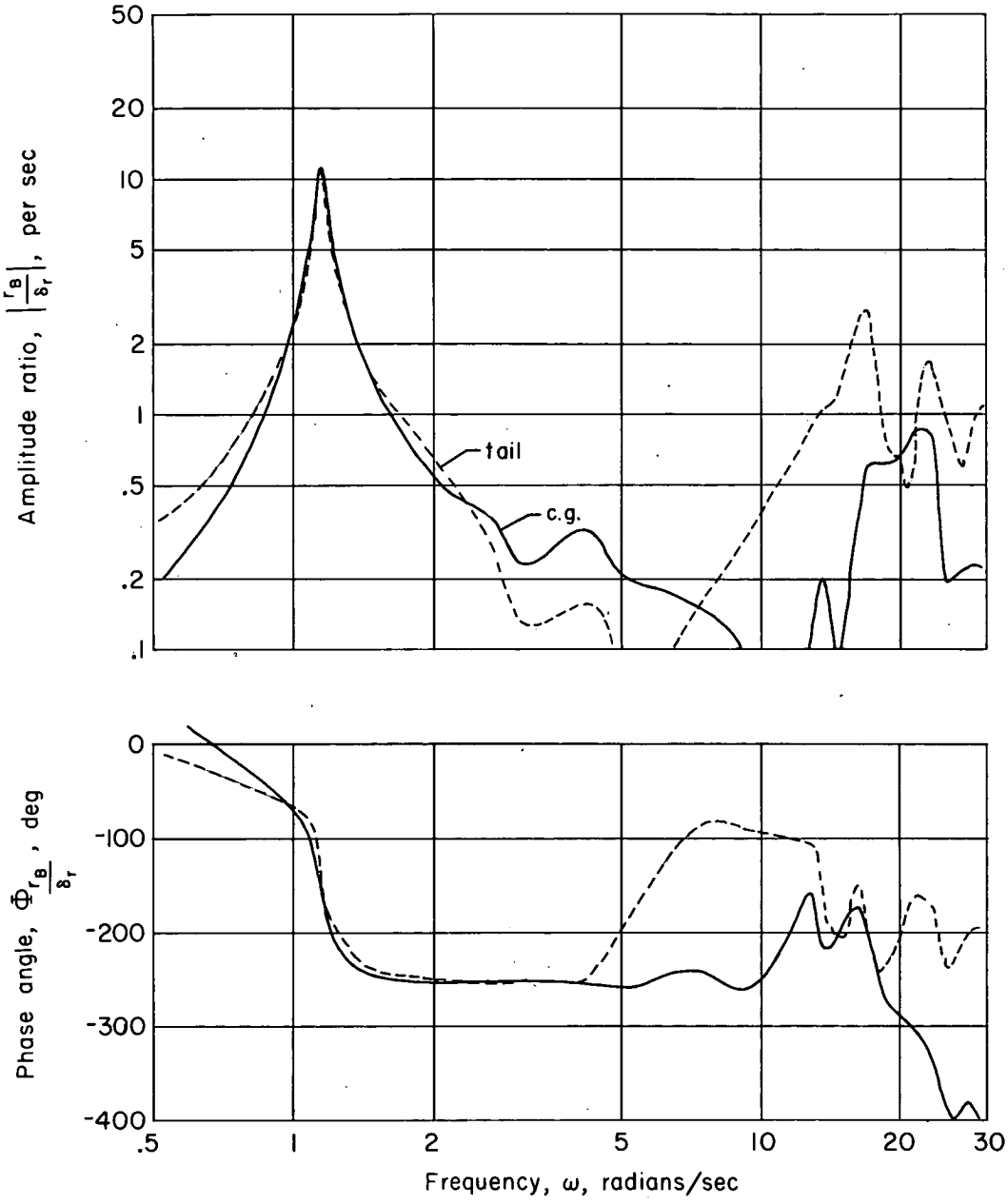

(b) Yawing velocity.

Figure 11.- Concluded.

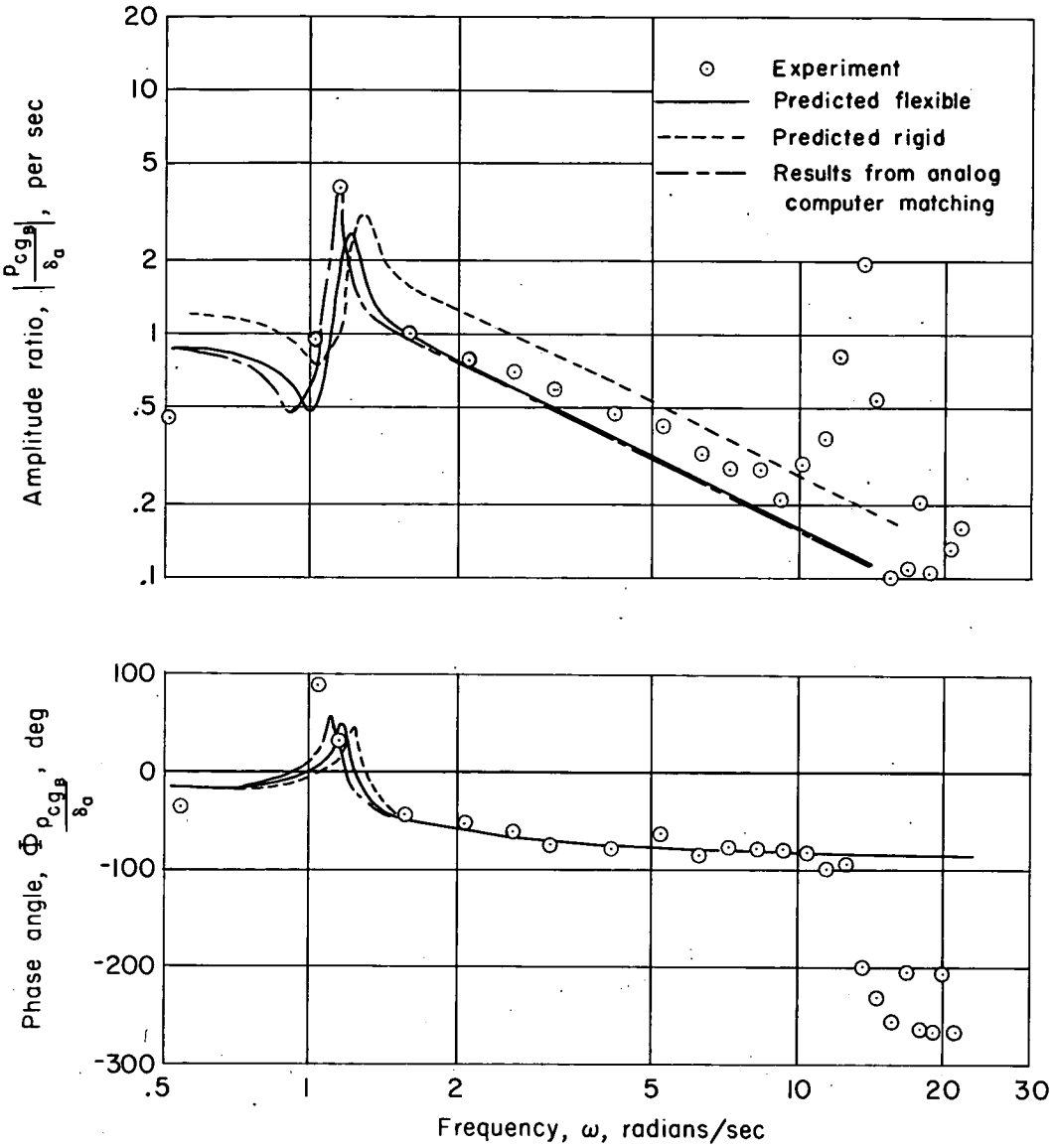

(a) Rolling velocity at the center of gravity.

Figure 12.- Comparison of experimental and predicted frequency responses to aileron input; M = 0.71.

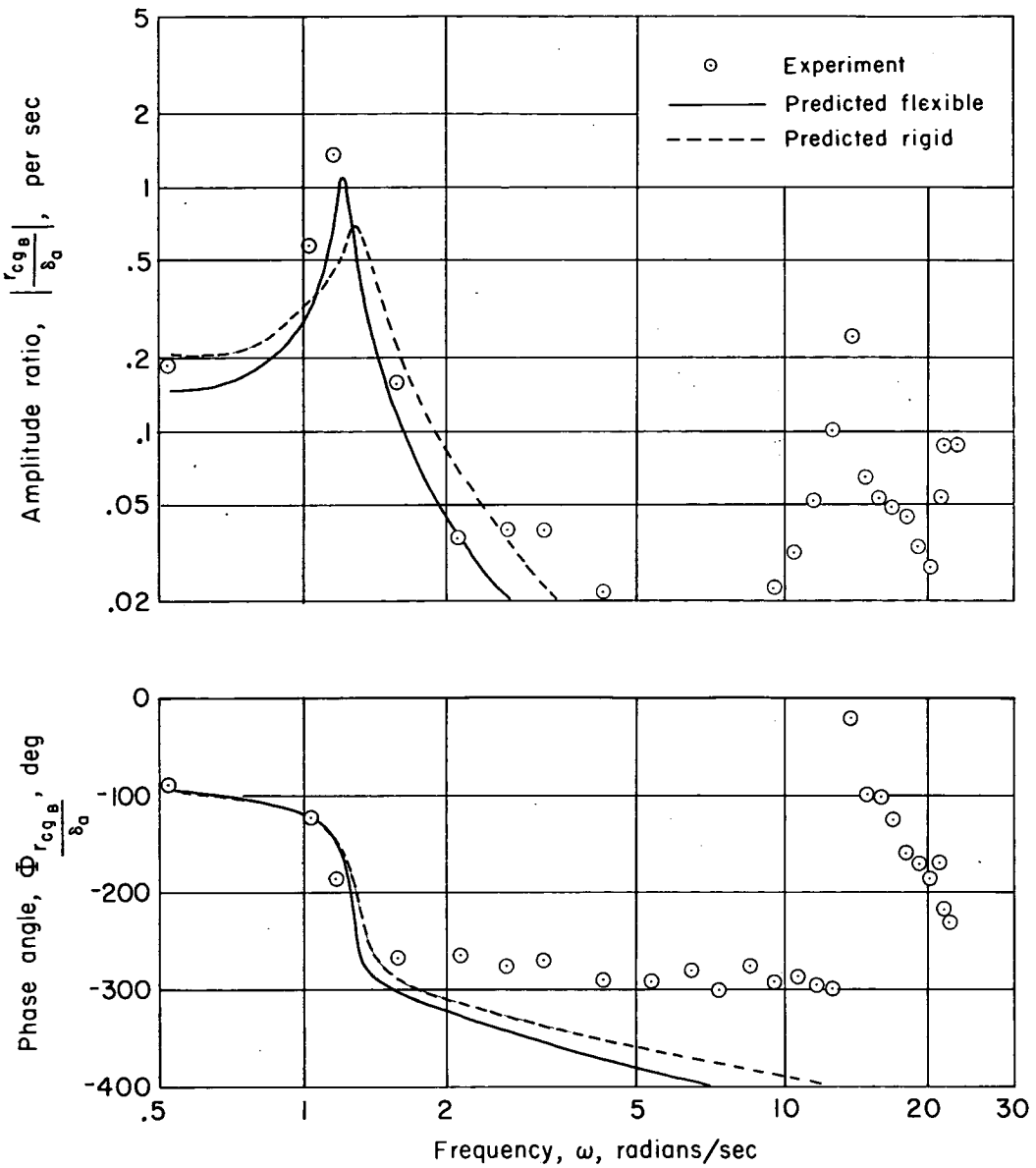

(b) Yawing velocity at the center of gravity.

Figure 12.- Continued.

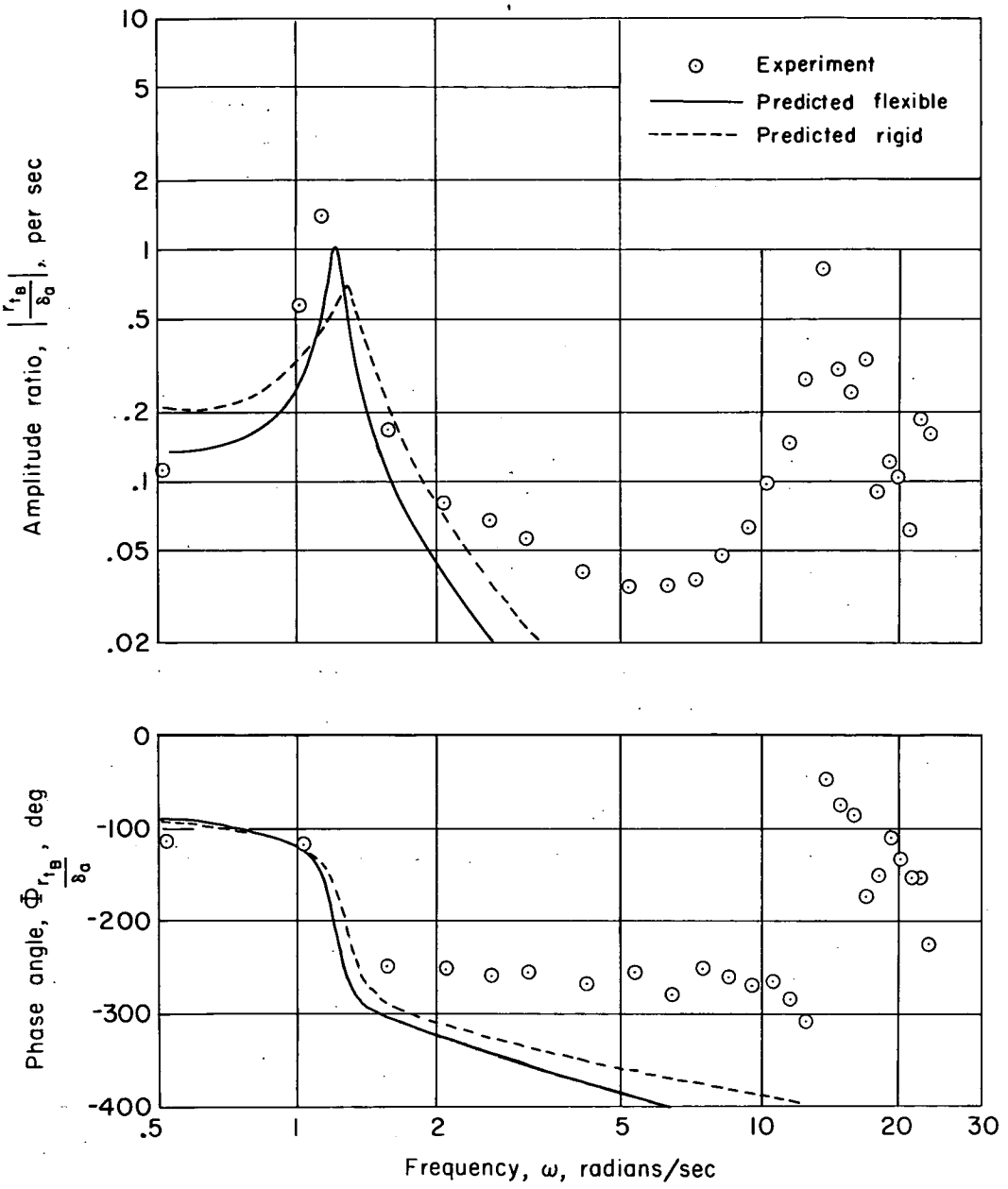

(c) Yawing velocity at the tail.

Figure 12.- Continued.

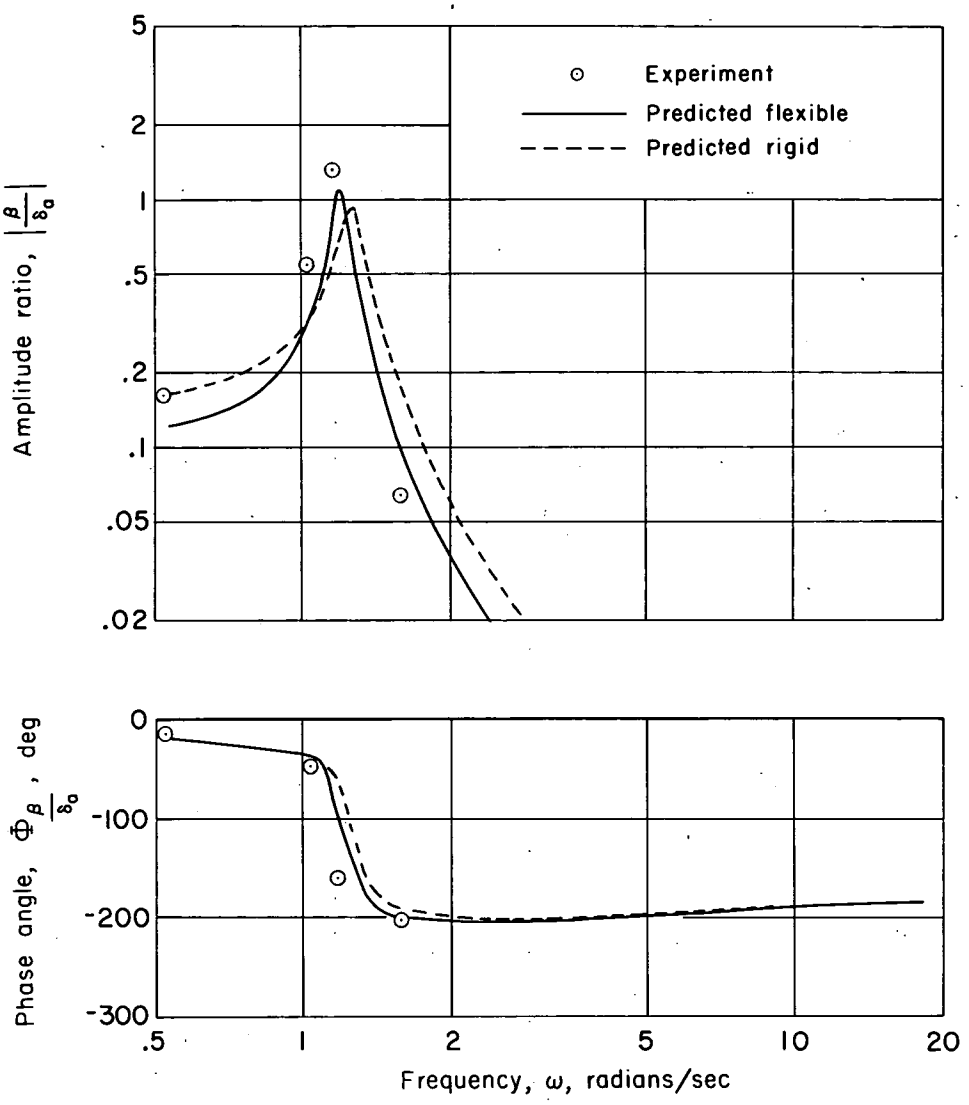

(d) Sideslip angle.

Figure 12.- Continued.

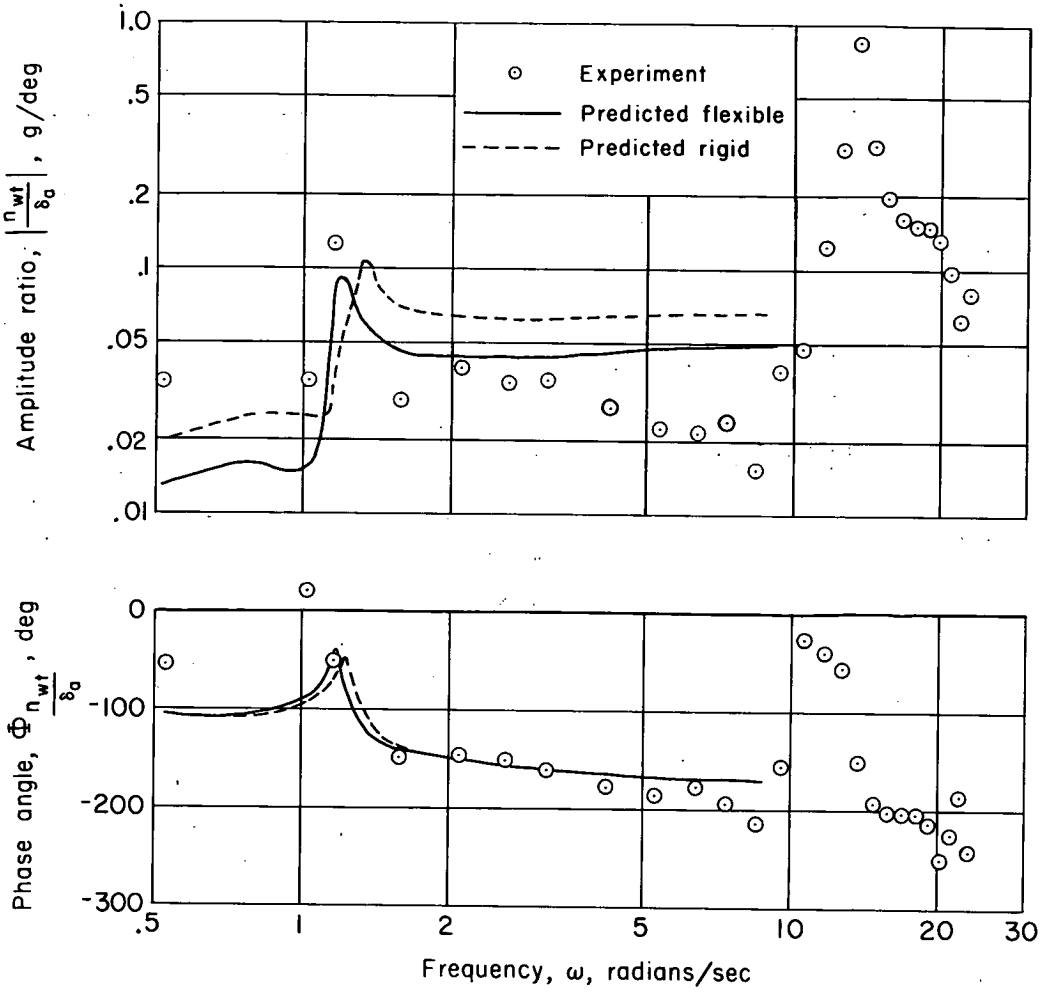

(e) Wing-tip acceleration.

Figure 12.- Concluded.

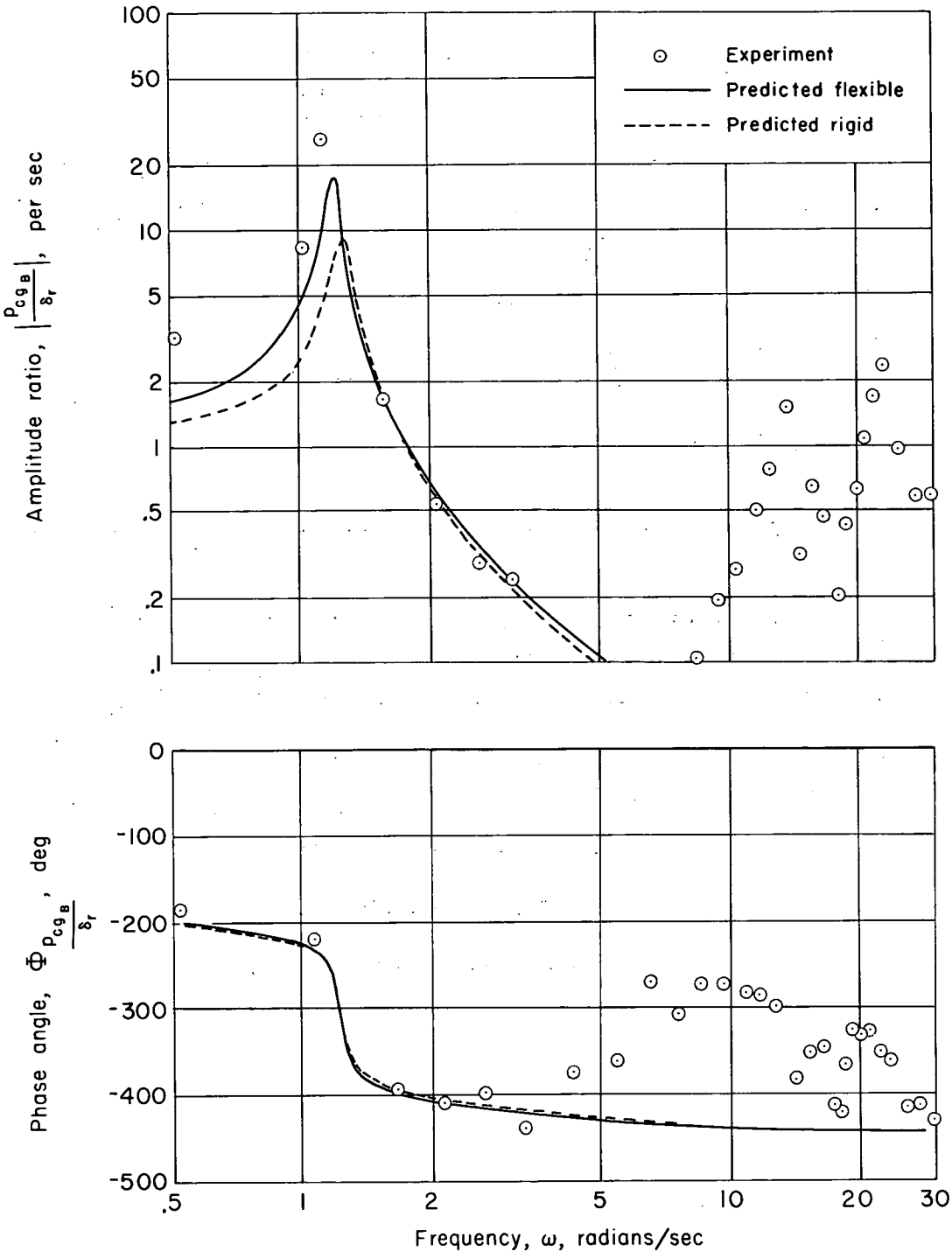

(a) Rolling velocity at the center of gravity.

Figure 13.- Comparison of experimental and predicted frequency responses to rudder input; M = 0.71.

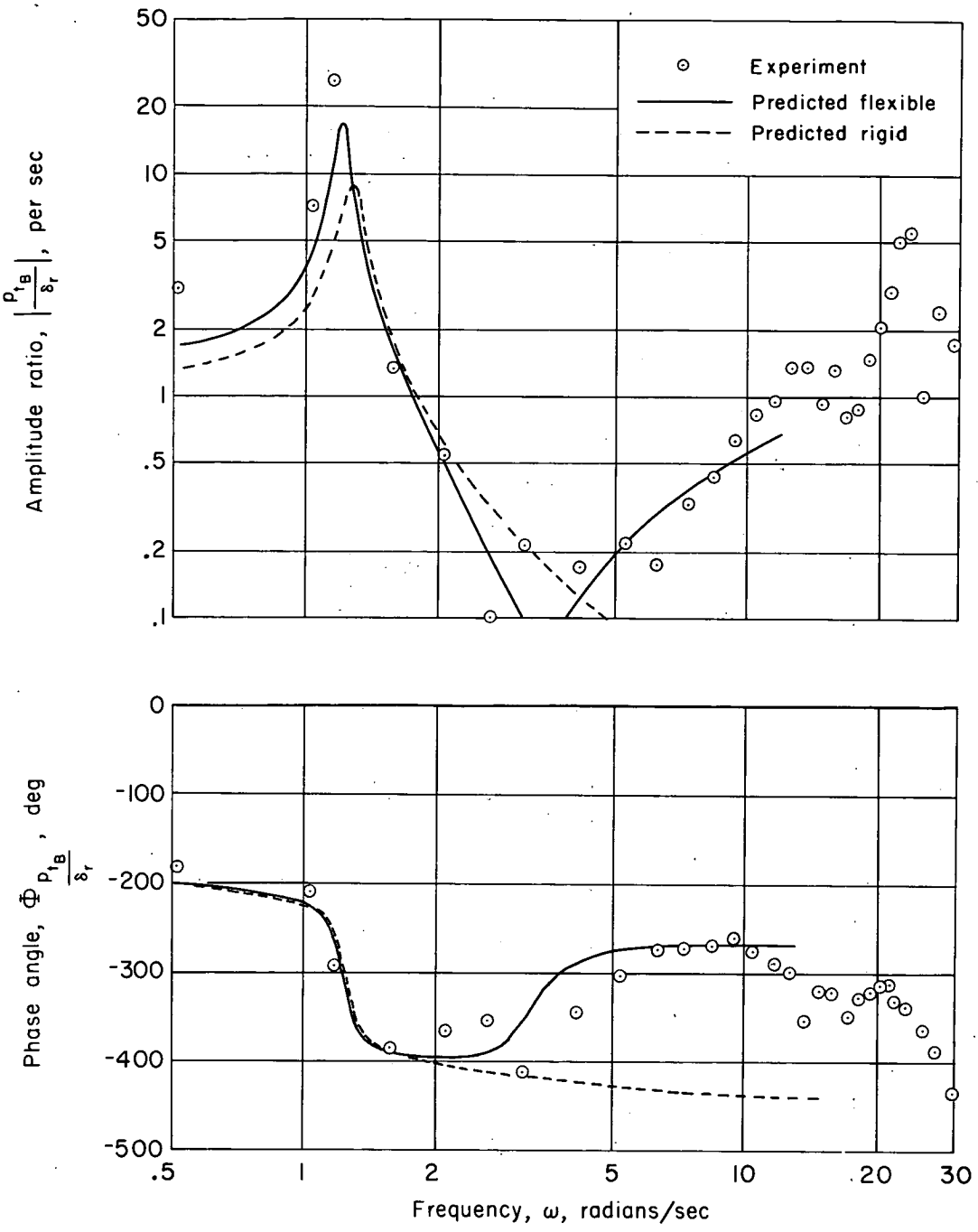

(b) Rolling velocity at the tail.

Figure 13.- Continued.

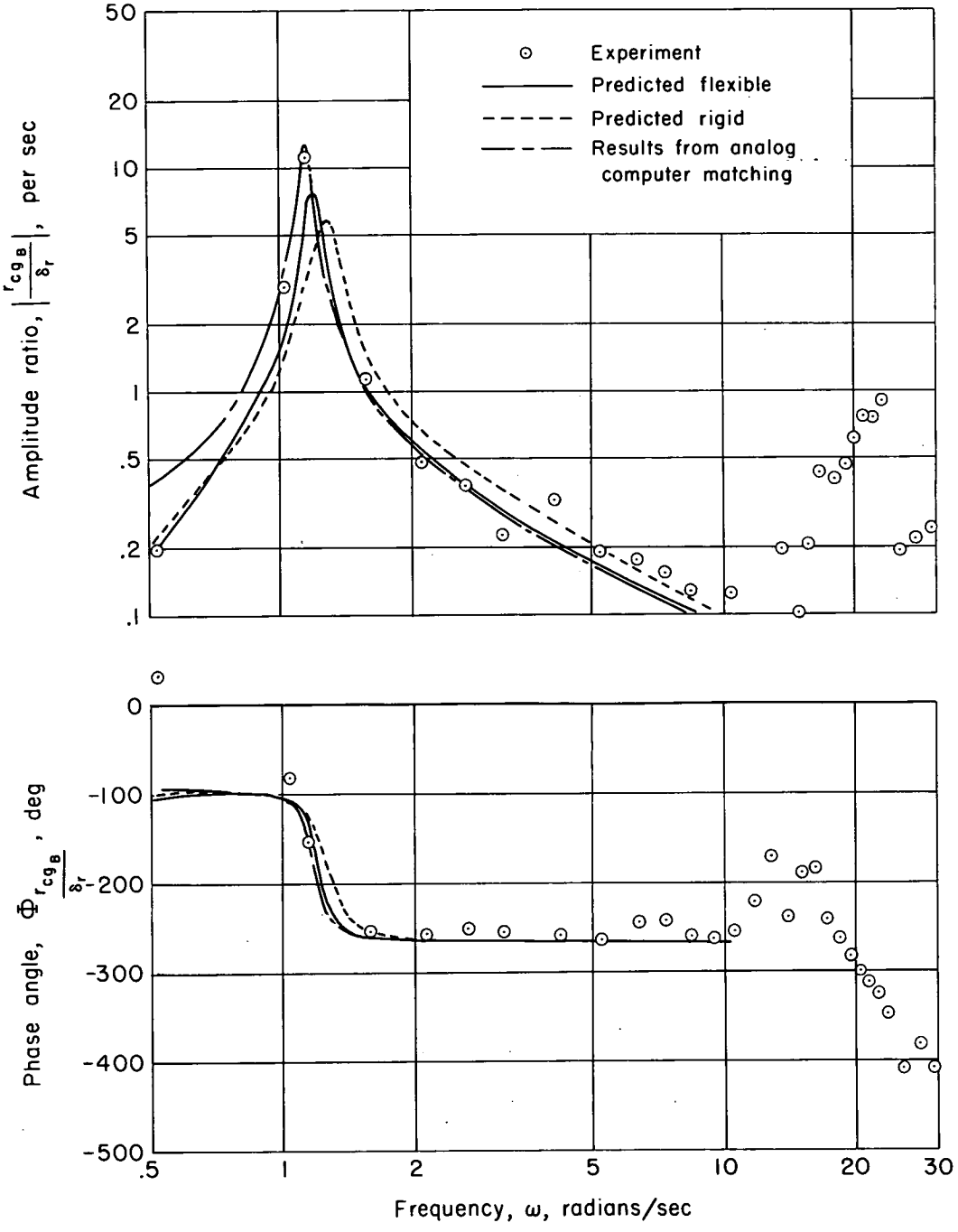

(c) Yawing velocity at the center of gravity.

Figure 13.- Continued.

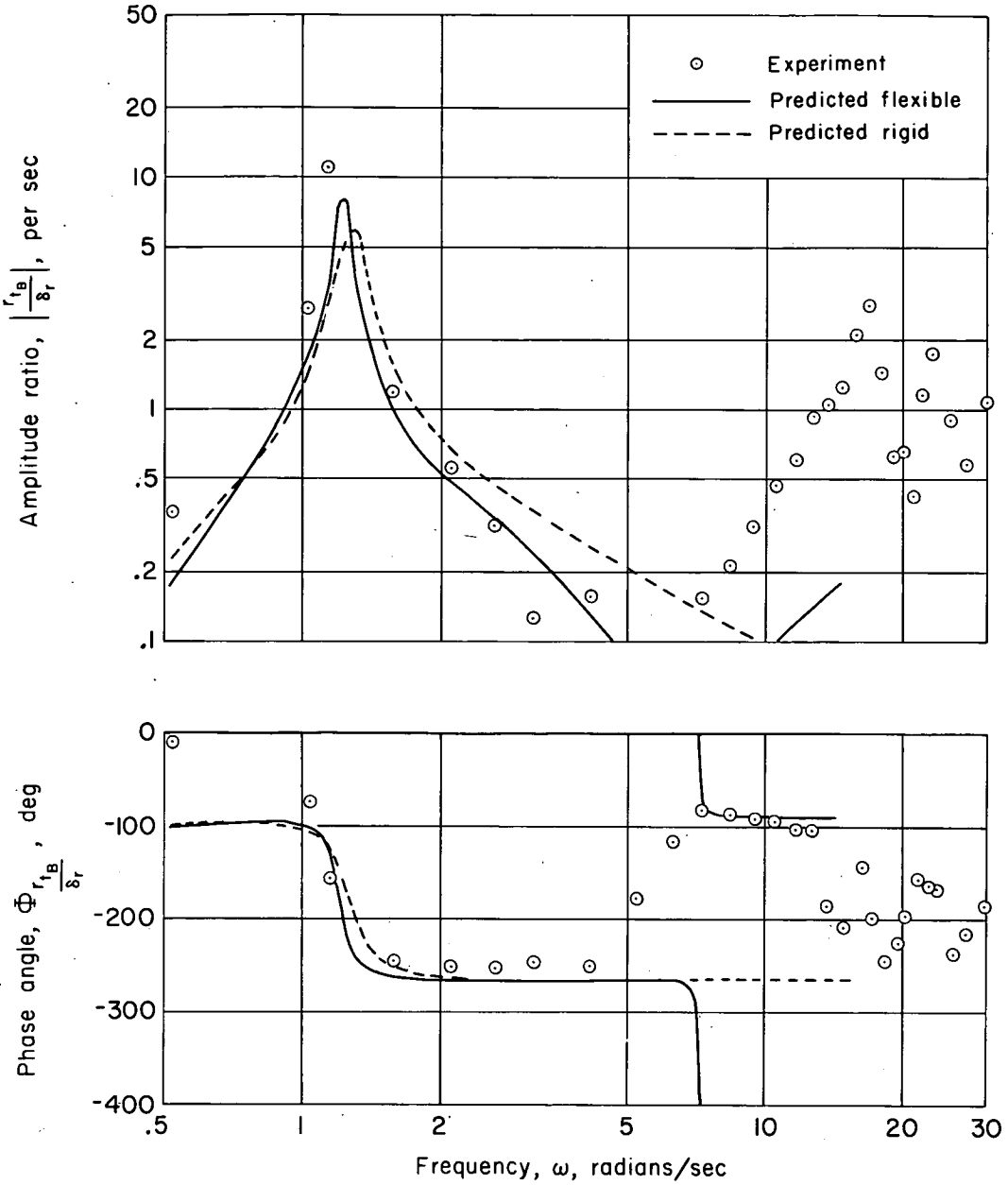

(d) Yawing velocity at the tail.

Figure 13.- Continued.

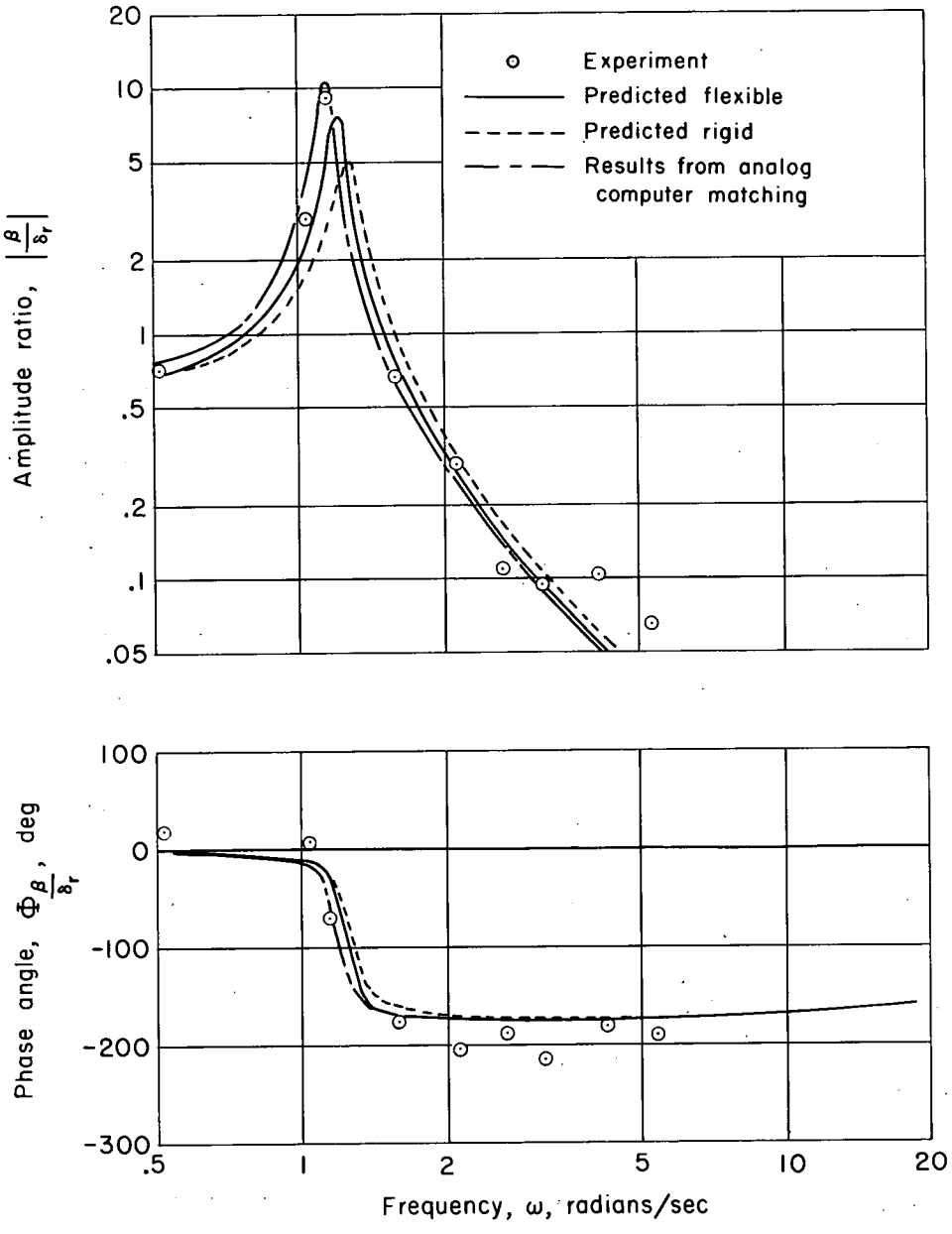

(e) Sideslip angle.

Figure 13.- Continued.

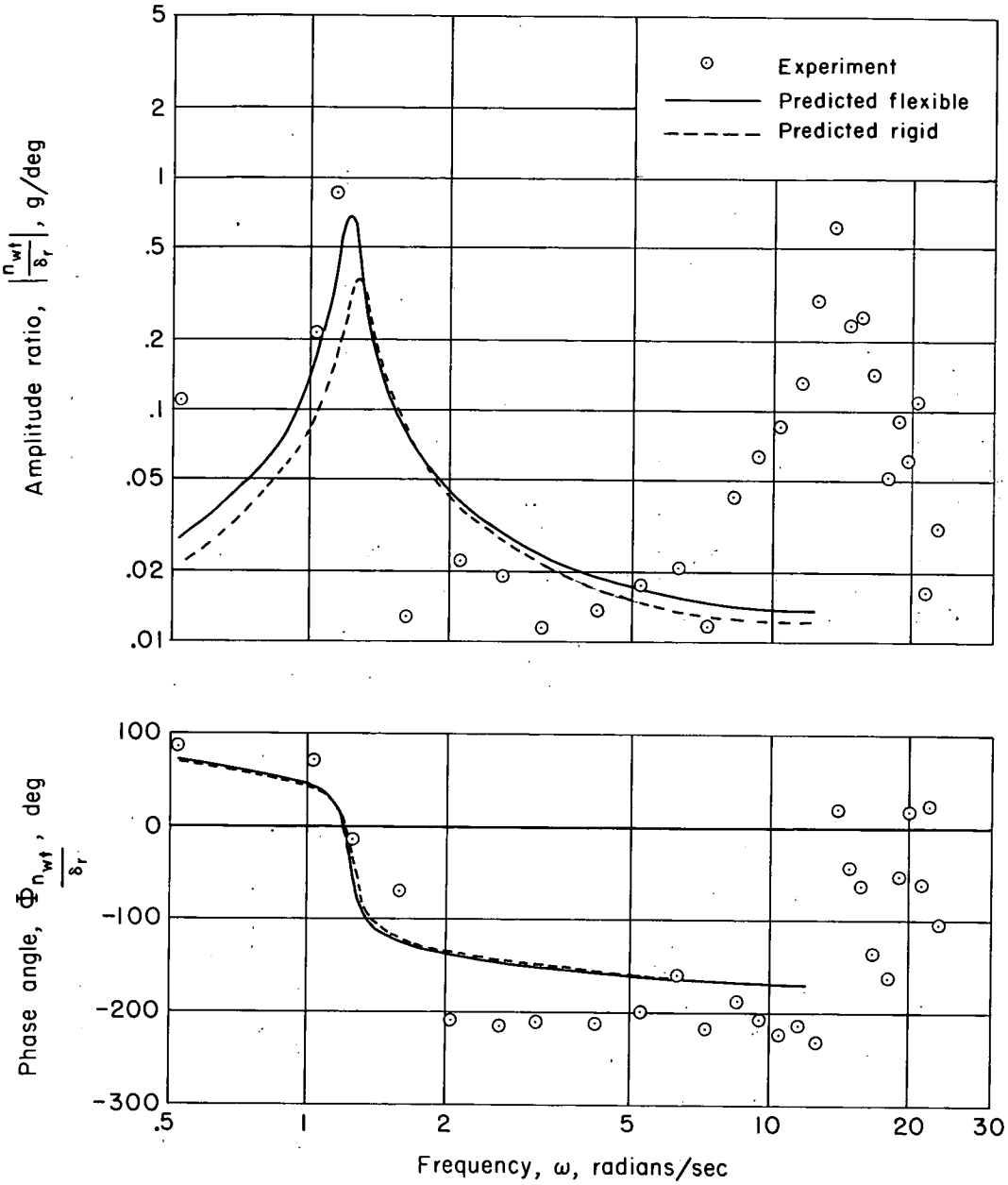

(f) Wing-tip acceleration.

Figure 13.- Concluded.

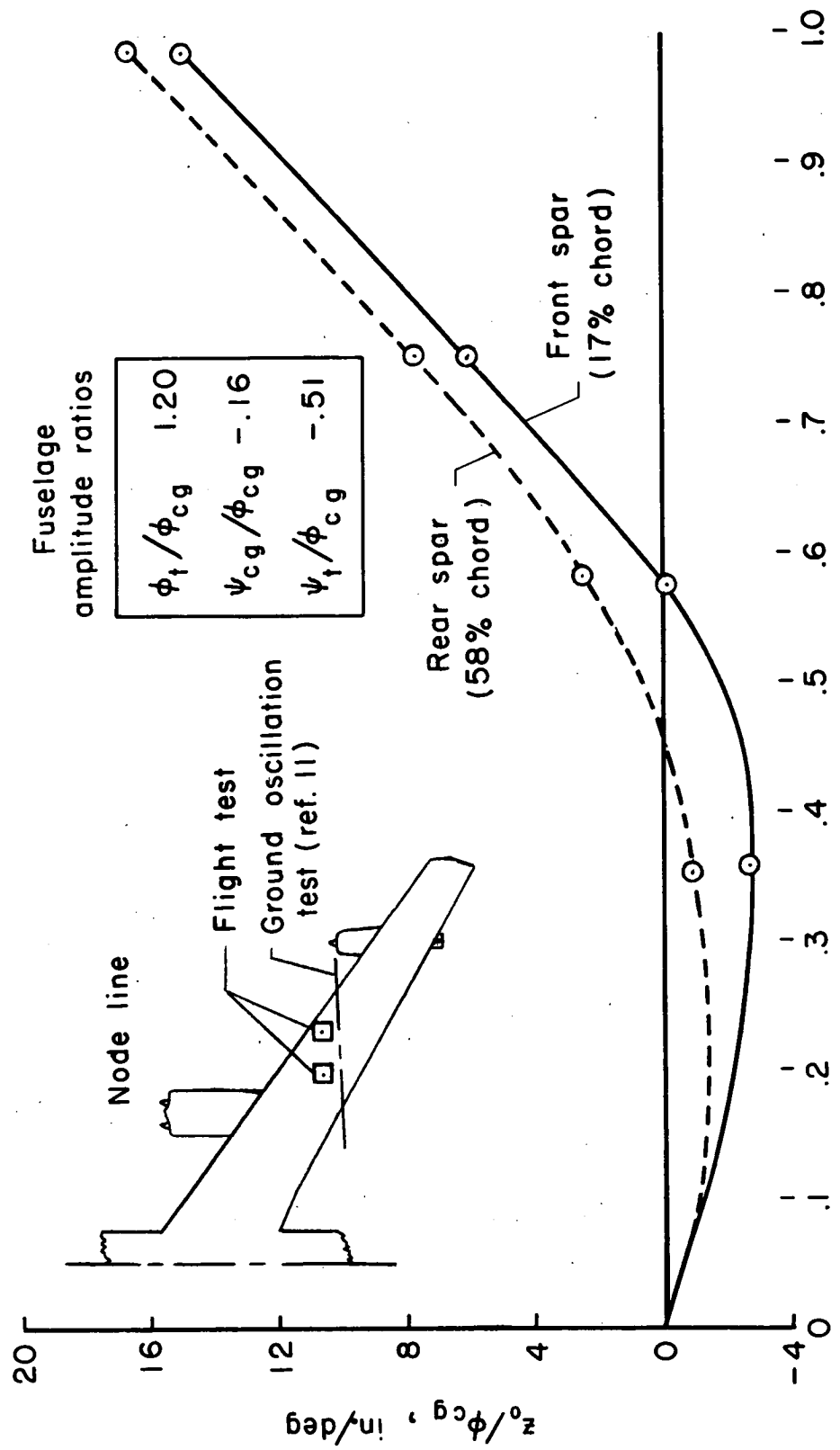

Figure 14.- First antisymmetric wing bending free oscillation mode shape; M = 0.71.

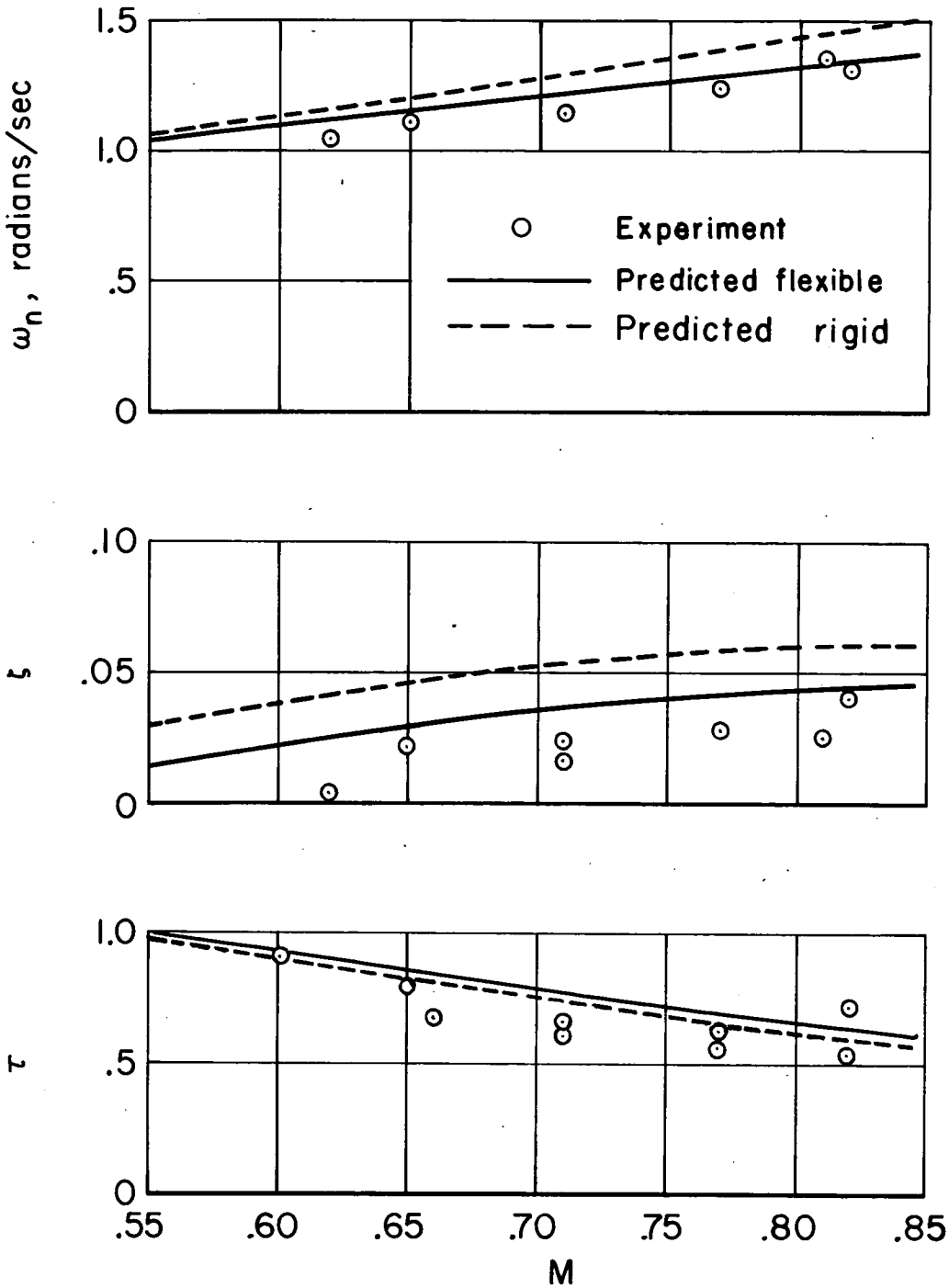

(a) Denominator coefficients.

Figure 15.- Comparison of experimental and predicted transfer-function coefficients.

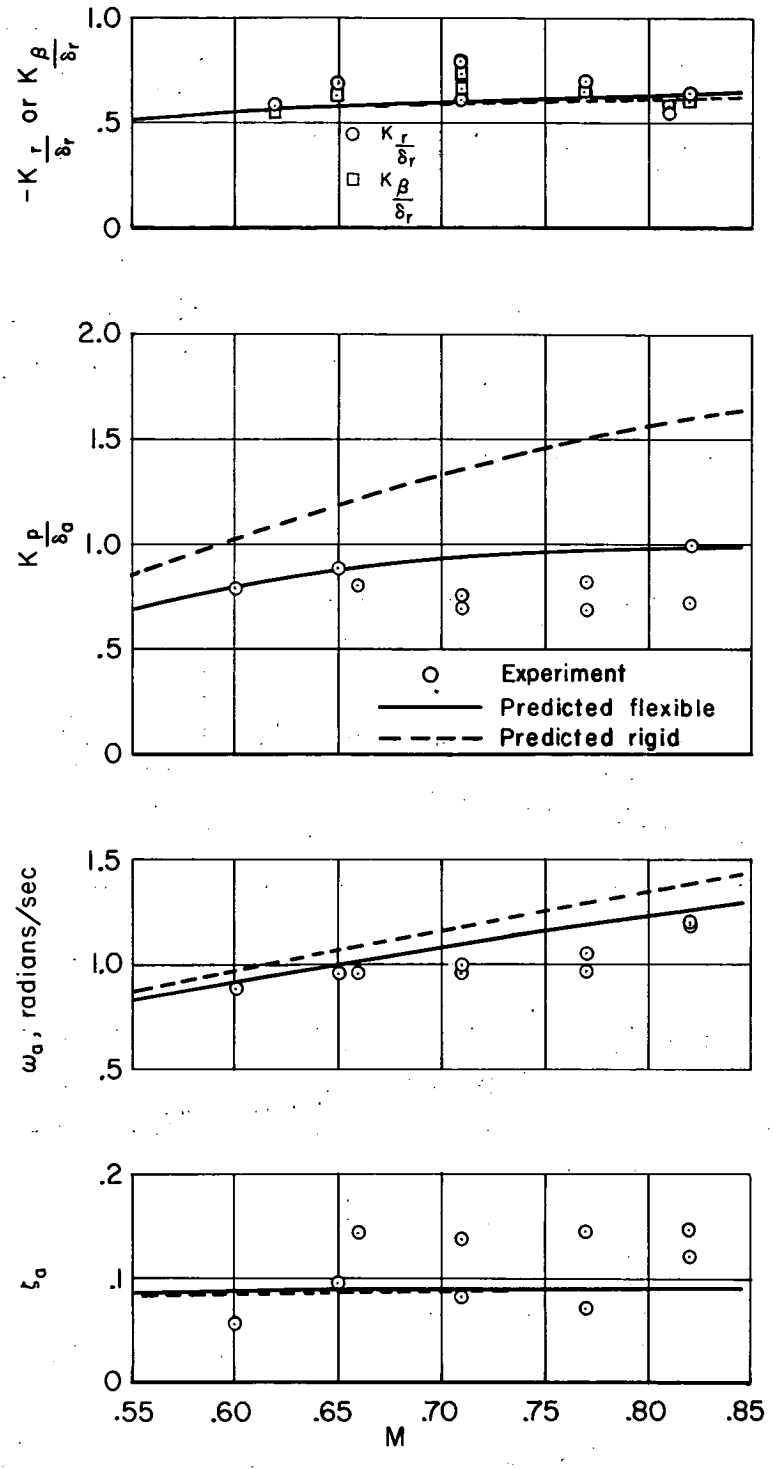

(b) Numerator coefficients.

Figure 15.- Concluded.

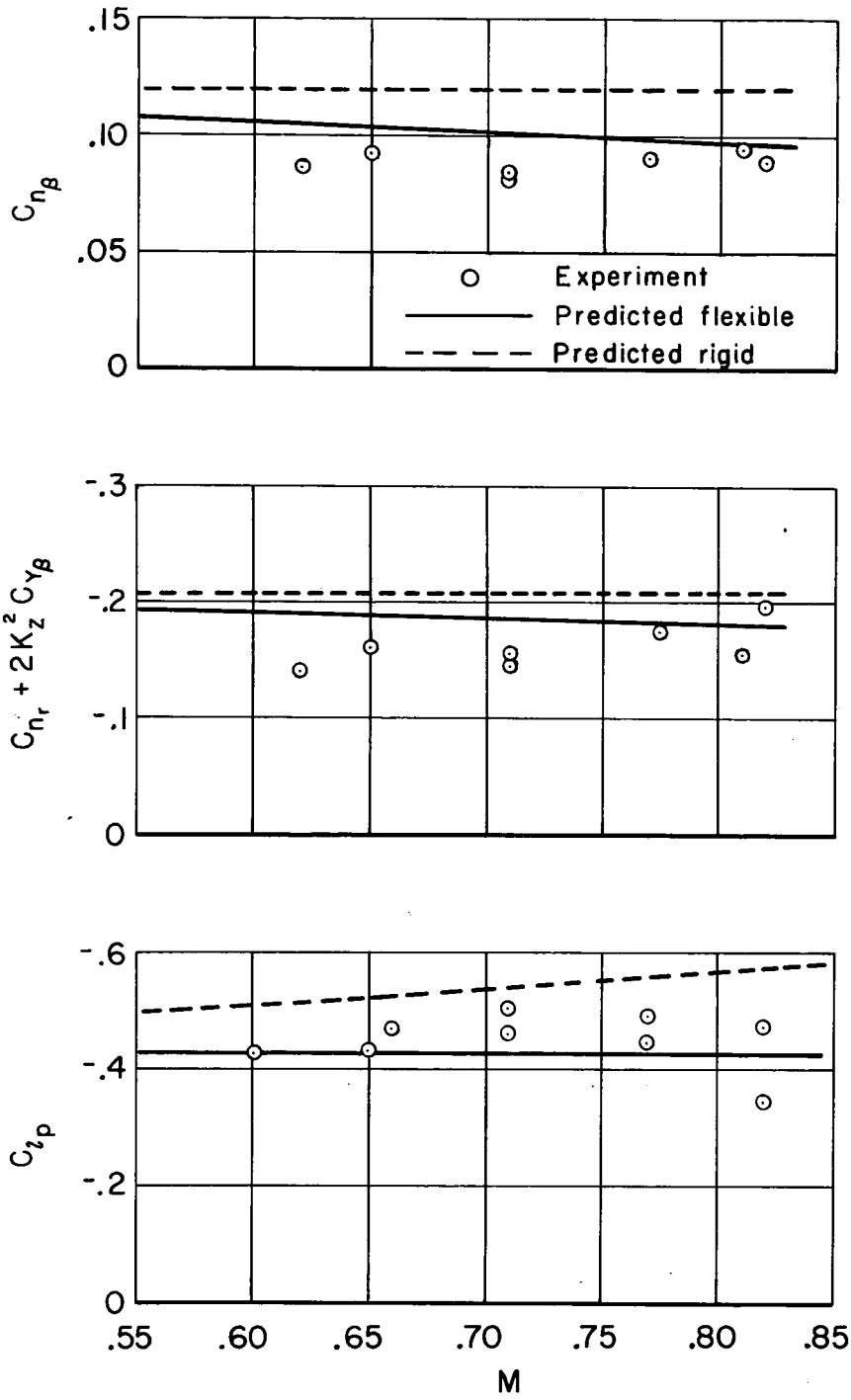

(a) The derivatives C_{n_β}, $C_{n_r} + 2K_Z{}^2 C_{Y_\beta}$, and C_{l_p}.

Figure 16.- Comparison of experimental and predicted aerodynamic derivatives.

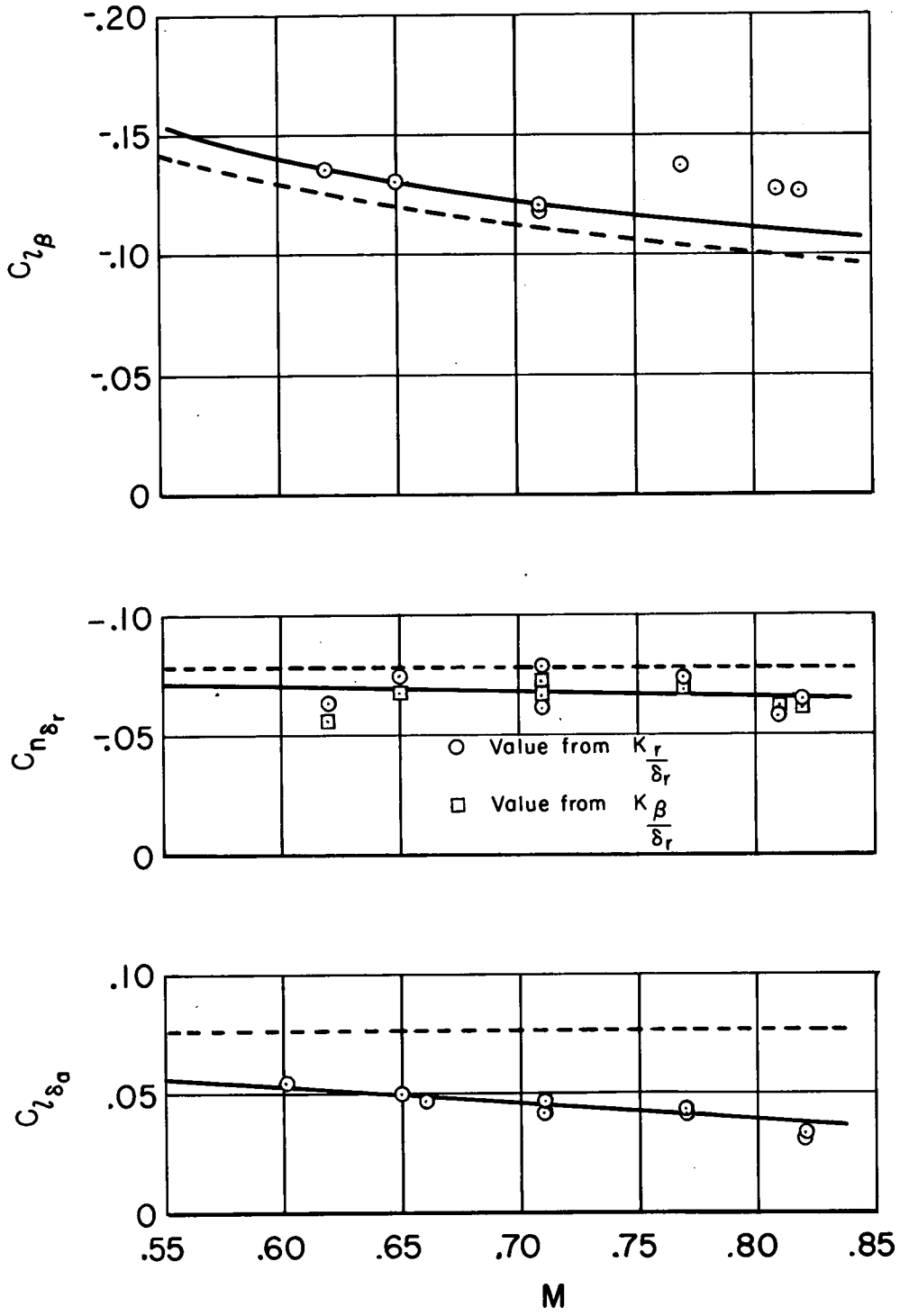

(b) The derivatives C_{l_β}, $C_{n_{\delta_r}}$, and $C_{l_{\delta_a}}$.

Figure 16.- Concluded.